Biogeosciences, 11, 1103–1123, 2014
www.biogeosciences.net/11/1103/2014/
doi:10.5194/bg-11-1103-2014

Biogeosciences Open Access

Subsurface pH and carbonate saturation state of aragonite on the Chinese side of the North Yellow Sea: seasonal variations and controls

W.-D. Zhai[1,2], N. Zheng[1], C. Huo[1], Y. Xu[2], H.-D. Zhao[1,2], Y.-W. Li[1,*], K.-P. Zang[1], J.-Y. Wang[1], and X.-M. Xu[1]

[1]Key Laboratory for Ecological Environment in Coastal Areas (State Oceanic Administration), National Marine Environmental Monitoring Center, Dalian 116023, China
[2]State Key Laboratory of Marine Environmental Science, Xiamen University, Xiamen 361102, China
[*]now at: College of Chemistry and Chemical Engineering, Taishan University, Tai'an 271000, China

Correspondence to: W.-D. Zhai (wdzhai@126.com)

Received: 31 December 2012 – Published in Biogeosciences Discuss.: 19 February 2013
Revised: 13 December 2013 – Accepted: 12 January 2014 – Published: 26 February 2014

Abstract. Based upon eight field surveys conducted between May 2011 and May 2012, we investigated seasonal variations in pH, carbonate saturation state of aragonite (Ω_{arag}), and ancillary data on the Chinese side of the North Yellow Sea, a western North Pacific continental margin of major economic importance. Subsurface waters were CO_2-undersaturated in May and nearly in equilibrium with atmospheric CO_2 in June. From July to October, the fugacity of CO_2 (fCO_2) of bottom water gradually increased from 438 ± 44 µatm to 630 ± 84 µatm, and pH_T decreased from 8.02 ± 0.04 to 7.88 ± 0.06 due to local aerobic remineralization of primary-production-induced biogenic particles. The subsurface community respiration rates in summer and autumn were estimated to be from 0.80 to 1.08 µmol-O_2 kg^{-1} d^{-1} within a relatively high salinity range of 31.63 to 32.25. From November to May in the next year, however, subsurface fCO_2 gradually decreased and pH increased due to cooling and water column ventilation. The corresponding bottom water Ω_{arag} was 1.85 ± 0.21 (May), 1.79 ± 0.24 (June), 1.75 ± 0.27 (July), 1.76 ± 0.29 (August), 1.45 ± 0.31 (October), 1.52 ± 0.25 (November), and 1.41 ± 0.12 (January). Extremely low Ω_{arag} values (from 1.13 to 1.40) were observed mainly in subsurface waters within the high salinity range of 31.63 to 32.25, which covered a major fraction of the study area in October and November. Of the China seas, the North Yellow Sea represents one of the systems most vulnerable to the potential negative effects of ocean acidification.

1 Introduction

Both pH and $CaCO_3$ saturation state (Ω) are essential parameters for the health of aquatic environments. Here pH is the negative logarithm of the total concentration of H^+ and HSO_4^- ions, i.e. $pH_T = -\log_{10}[H^+]_T$, where $[H^+]_T = [H^+] + [HSO_4^-]$. It affects chemical/biochemical properties of seawater, including chemical reactions, equilibrium conditions, and biological toxicity. In response to increasing atmospheric CO_2, the effect of decreasing pH has received considerable attention during the past decade (e.g. Caldeira and Wickett, 2003; Orr et al., 2005; Doney et al., 2009; Duarte et al., 2013).

Ω is defined as the product of calcium and carbonate ion concentrations divided by the apparent solubility product (K^*_{sp}) of calcium carbonate, i.e. $\Omega = [Ca^{2+}][CO_3^{2-}]/K^*_{sp}$. Without protective mechanisms, calcifying organisms are vulnerable to corrosive $CaCO_3$-undersaturated seawaters with $\Omega < 1$ (Feely et al., 2002, 2008; Yamamoto-Kawai et al., 2009; Gruber et al., 2012).

$CaCO_3$ occurs in marine environments as three polymorphs, i.e. calcite, aragonite and magnesian calcite. Pure calcite (> 99 mol% $CaCO_3$) is more stable than aragonite, while high-Mg calcite (> 12 mol% $MgCO_3$) is more soluble than aragonite (Morse et al., 2006, 2007; Woosley et al., 2012). Since aragonite is usually the most abundant carbonate mineral in shallow sea areas (Morse et al., 2006), we adopted the carbonate saturation state of aragonite (Ω_{arag}) to measure its potential to corrode $CaCO_3$ shells and skeletons

of marine organisms. In the Pacific Ocean, the present surface Ω_{arag} values are 1 to 2 in high-latitude regions and 3 to 4.5 in low-latitude regions (Feely et al., 2012). In high-latitude regions, sea surface waters absorb a considerable amount of CO_2 from the atmosphere due to the high solubility of CO_2 at low temperatures, leading to low Ω_{arag} values. Marine calcifying organisms may require a Ω_{arag} much higher than 1 for optimal growth (Shamberger et al., 2011), while carbonate biominerals in calcic shells and skeletons may undergo dissolution even at relatively high levels of Ω_{arag} (between 3.0 and 3.2) (Yamamoto et al., 2012). This is partially because, in present oceans with seawater Ca : Mg molar ratios of about 1 : 5 (Steuber and Rauch, 2005), many carbonate biominerals are composed of instable high-Mg calcite (Morse et al., 2006, 2007; Long et al., 2011).

Low pH and Ω_{arag} values may occur in coastal zones due to local oceanographic processes, e.g. coastal upwelling and water mixing with fresh waters (Feely et al., 2008, 2010; Salisbury et al., 2008; Yamamoto-Kawai et al., 2009; Gruber et al., 2012), metabolic processes (Feely et al., 2010; Taguchi and Fujiwara, 2010; Cai et al., 2011; Zhai et al., 2012), and regional environmental changes, such as eutrophication (Borges and Gypens, 2010; Sunda and Cai, 2012). In eutrophicated regions, algal blooms and red tides absorb CO_2 on the sea surface, producing large amounts of sinking organic matter, which is remineralized below the euphotic depth (e.g. Feely et al., 2010; Taguchi and Fujiwara, 2010; Cai et al., 2011; Zhai et al., 2012). The aerobic remineralization process can be roughly characterized by the Redfield equation (Redfield et al., 1963):

$$(CH_2O)_{106}(NH_3)_{16}H_3PO_4 + 138O_2 \rightarrow 106CO_2 + 16HNO_3 + H_3PO_4 + 122H_2O. \quad (1)$$

Clearly, the release of CO_2 increases carbonic acid levels in subsurface waters. If local hydrodynamic conditions do not enable outgassing of subsurface CO_2, a significant pH decrease (by 0.2 to 0.3 units) can occur on seasonal or shorter time scales (e.g. Taguchi and Fujiwara, 2010; Cai et al., 2011; Zhai et al., 2012). These seawater acidification processes may threaten marine calcifying species (e.g. Gao et al., 1993; Green et al., 2009; Dias et al., 2010; Liu and He, 2012; Andersen et al., 2013; Xu et al., 2013) and even non-calcifying species (e.g. Munday et al., 2009, 2010; Baumann et al., 2012; Briffa et al., 2012; Domenici et al., 2012).

So far, only a few mechanistic studies have been conducted to investigate the dynamics of pH and Ω in continental margins of eastern Asia (Cao et al., 2011; Zhai et al., 2012; Chou et al., 2013), although this region sustains numerous commercially valuable and acidification-sensitive fisheries, e.g. of bivalve molluscs and crustaceans. Surrounding the North Yellow Sea (NYS), the Liaoning and Shandong provinces of China are teeming with fast-developing marine aquaculture activities, and are highly populated (Fig. 1). Acidification-sensitive bivalve molluscs of the family Pectinidae and echinoderms of the class Holothuroidea are of major ecological and economic importance in these NYS coastal ecosystems. Scallop-breeding failures have occasionally been reported in this region (Du et al., 1996). Thus far, however, information regarding pH and Ω in this region remains limited. We investigated seasonal variations in pH and Ω_{arag} on the Chinese side of the NYS, revealing controls of subsurface pH and Ω_{arag} dynamics in this continental margin. This high-quality Ω_{arag} data set is the first reported for this important marine aquaculture region.

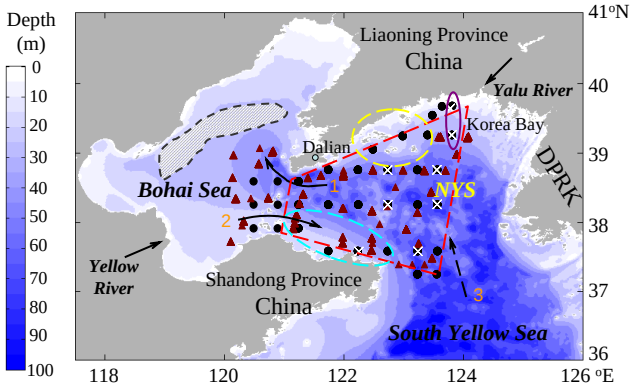

Fig. 1. North Yellow Sea (NYS) together with the Bohai Sea and sampling sites. The study focused on the area enclosed within the red polygon. A major marine aquaculture zone in the NYS is enclosed within the yellow ellipse. Closed circles mark stations that were sampled in May, July, and October 2011. Triangles mark stations that were sampled in June, August, and November 2011, and May 2012. White crosses mark stations that were sampled in January 2012. The Bohai Sea inflow current (1), Bohai Sea outflow current (2) and wintertime Yellow Sea Warm Current (3) were modified from Chen (2009). Two northern stations enclosed by the purple ellipse were subject to frozen temperatures during the January cruise. Several southwest stations enclosed by the blue ellipse were likely influenced by the outflow of Bohai Sea water. A bottom-water oxygen-depletion region in August 2011 in the Bohai Sea is sketched with the grey shadowed area (Zhai et al., 2012).

2 Materials and methods

2.1 Study area

The NYS is a shallow marginal sea of the western North Pacific, surrounded by Liaoning and Shandong provinces of China and the Democratic People's Republic of Korea (Fig. 1), with an area of 71 300 km^2 and a mean depth of 38 m (He and Yu, 2013). Climatic variations of the NYS are primarily dominated by the East Asian Monsoon (Chen, 2009). The rain-bearing southwest monsoon lasts from June to September (Fig. 2a), while the strong northeast monsoon prevails in winter, from November to March of the next year.

The NYS is connected to the Bohai Sea through a relatively narrow channel, whereas it is more open to the South Yellow Sea (SYS) (Fig. 1). In addition to the

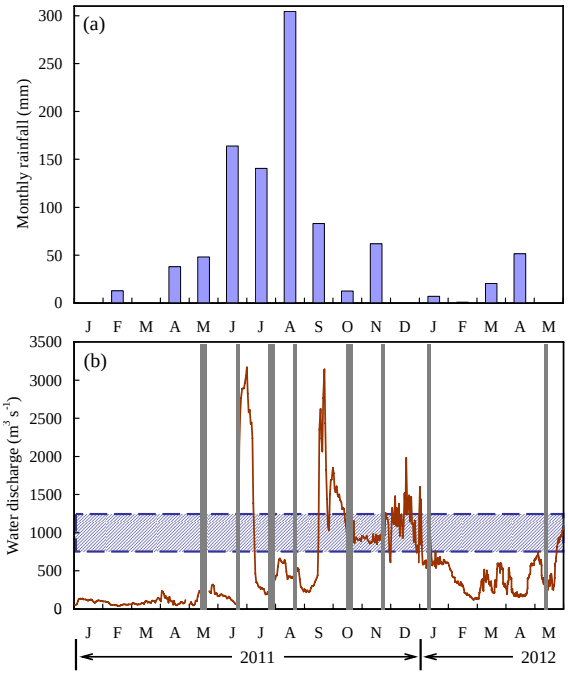

Fig. 2. Monthly rainfall in the study area **(a)**; real-time water discharge from the Yellow River into the Bohai Sea (brown line) from January 2011 to May 2012 **(b)**. The usual variation range of water discharge from Yalu River is shown by the indigotic shadowed area in panel **(b)**, based on real-time data between September 2012 and July 2013. All data are from the China Bureau of Hydrology (http://xxfb.hydroinfo.gov.cn/). Vertical grey columns show surveying periods.

600 to 800 mm yr^{-1} of rainfall (Zhang, 1994; Fig. 2a), the NYS is fed by freshwater discharge of approximately 33×10^9 m^3 yr^{-1} from Yalu River (Liu and Liu, 1992; Zhang, 1996; Zhang et al., 1997), with the runoff having a relatively low alkalinity of approximately 740 µmol kg^{-1} (Zhang, 1997). Due to these freshwater inputs, the typical NYS water mass has a relatively low salinity (31.50 to 32.50) (Miao et al., 1991; Chen, 2009) compared with open oceans. The general circulation in the NYS is a nearly year-round weak counter clockwise gyre (Fig. 1; Miao et al., 1991; Zhao, 1996; Qiao et al., 1998). The summertime hydrography across the NYS is characterized by a pronounced stratification in the deeper region. A cold pool, typically 5 to 11 °C, is overlain by 20 to 25 m of warm water (Miao et al., 1991; Chen, 2009), which is regarded as the remnant of winter cooling and documented as the NYS cold water mass (NYSCWM; Miao et al., 1991; Zhao, 1996; Qiao et al., 1998). Wintertime circulation is characterized by the Yellow Sea Warm Current (YSWC), which is considered a compensating current of the northeast monsoon driven coastal currents (Hsueh, 1988; Yuan et al., 2008), transporting saline SYS water to the NYS (Fig. 1; Chen, 2009).

The high frequency of algae blooms has been noted in the past 30 yr (Zhang, 1994; State Oceanic Administration of China, 2012). Besides the limited effects of nutrient inputs from Yalu River (Zhang et al., 1997), both atmospheric deposition of nutrient elements and nutrient regeneration from benthic processes may have significant impacts upon phytoplankton growth in the NYS (Zhang, 1994; Zhang et al., 2002; Tan et al., 2011). The atmospheric CO_2 concentration in 2011 fluctuated from 383 ppmv (parts per million volume in dry air) in late July to 408 ppmv in mid-May and mid-November according to flask analyses at the adjacent Tae-ahn Peninsula (TAP) site (36°44′ N 126°08′ E), and had an annual average of 398 ppmv (data from NOAA/ESRL's Global Monitoring Division, http://www.esrl.noaa.gov/gmd/).

The western and central parts of the NYS (study area) exchange water and other materials with the semi-enclosed Bohai Sea (Fig. 1). The Bohai Sea has a volume of 1.4×10^{12} m^3 (Wei et al., 2002; Chen, 2009) and a very long water exchange half-life of 17 to 21 months (Wei et al., 2002). It is fed by more than a dozen rivers of moderate or high alkalinity (1470 to 6300 µmol kg^{-1}) (Wang et al., 2005; Xia and Zhang, 2011), including major runoff contributions from the Yellow River. During the past 60 yr, annual water discharge from the Yellow River has significantly declined; it was $50 \pm 20 \times 10^9$ m^3 yr^{-1} in the 1950s and 1960s, and only 5×10^9 m^3 yr^{-1} in the late 1990s (Wu et al., 2004; Wang et al., 2007). Over the last 10 yr, annual water discharge from the lower Yellow River has been manipulated at approximately 20×10^9 m^3 yr^{-1} (based on daily water discharge data from the China Bureau of Hydrology, http://xxfb.hydroinfo.gov.cn/). These remarkable freshwater and alkalinity fluxes circulate in the Bohai Sea for more than 1.5 yr (Wei et al., 2002; Mao et al., 2008), supporting the relatively homogeneous low salinity of 30.50 to 31.50 (Chen, 2009; Zhai et al., 2012) and relatively high alkalinity (∼ 2400 µmol kg^{-1}, this study). Therefore, the outflow of Bohai Sea water (Fig. 1) can serve as an alkalinity source in the study area.

2.2 Survey design

Between May 2011 and May 2012, eight field surveys (Table 1) were conducted in late spring (May), early summer (June), mid-summer (July), late summer (August), autumn (October and November) and winter (January). This hydrological year was characterized by a wet summer (total rainfall of ∼ 610 mm in June, July, and August 2011) and a dry winter (total rainfall of ∼ 10 mm in December 2011, January 2012, and February 2012) (Fig. 2a). Both spring and autumn were transitional seasons between the wet summer and dry winter. However, water flow in the lower Yalu River was regulated by several major dams (including Sup'ung, Yunfeng, Weiyuan, and Taipingwan), usually varying little within a narrow range of 1000 ± 250 m^3 s^{-1} (Fig. 2b).

Table 1. Summary of the sampling cruises.

Surveying period	R/V	Stations in NYS	Field-measured data
10–17 May 2011	*Yixing*	26	*T*, *S*, TAlk, DIC, pH, chl *a*
22–24 Jun 2011	*Dongfanghong 2*	17	*T*, *S*, TAlk, DIC, pH, DO
24–31 Jul 2011	*Yixing*	24	*T*, *S*, TAlk, DIC, pH, chl *a*
20–22 Aug 2011	*Yixing*	16	*T*, *S*, TAlk, DIC, pH, DO
18–23 Oct 2011	*Yixing*	25	*T*, *S*, TAlk, DIC, pH, DO, chl *a*
22–25 Nov 2011	*Dongfanghong 2*	21	*T*, *S*, TAlk, DIC, pH, DO
9–13 Jan 2012	*Yixing*	8	*T*, *S*, TAlk, pH, DO, chl *a*
13–15 May 2012	*Dongfanghong 2*	23	*T*, *S*, TAlk, DIC

During these surveys, water samples were collected at 8 to 26 grid stations for pH, total alkalinity (TAlk), dissolved inorganic carbon (DIC), dissolved oxygen (DO), and chlorophyll *a* (chl *a*) testing (Table 1). Most sampling stations had a water depth of 25 to 78 m (Fig. 1). The northern sampling stations were near a highly developed marine aquaculture zone around Dalian City (Fig. 1). To examine the influences of the Bohai Sea water mass on the carbonate system in the study area, TAlk data collected in the eastern part of the Bohai Sea (Fig. 1) were also included in this study.

2.3 Sampling and analyses

Depth profiles of temperature and salinity (practical salinity scale of 1978) were determined with calibrated conductivity-temperature-depth/pressure (CTD) recorders (SBE911+ in June 2011, November 2011, and May 2012, and SBE19+ during other surveying periods, Sea-Bird Co., USA) aboard R/V *Dongfanghong* 2 (June 2011, November 2011, and May 2012) and R/V *Yixing* (other surveying periods). Water samples were obtained at three to four different depths using rosette samplers fitted with 8 L or 2.5 L Niskin bottles, which were mounted with CTD units. The bottom-water samples were collected from a depth of 2 to 5 m above the sea bed.

Water samples for DO analyses were collected, fixed, and titrated aboard following the classic Winkler procedure. A small quantity of NaN_3 was added during subsample fixation to remove possible interference from nitrites (Wong, 2012). Based on repeat determinations of the $Na_2S_2O_3$ titration reagent concentration, the uncertainty of the DO data was estimated to be at the satisfactory level of < 0.5 % (Zhai et al., 2012). The DO saturation (DO%) was calculated from the field-measured DO concentration divided by the DO concentration at equilibrium with the atmosphere, as per the Benson and Krause (1984) equation and the standard sea surface barometric pressure (i.e. 1.013×10^5 Pa).

Water samples for pH analyses were collected in 140 mL brown borosilicate glass bottles using a procedure similar to that used for DO. They were preserved with 50 µL saturated $HgCl_2$, sealed with screw caps, and measured at 25.0 °C within 6 h of sampling. The precision pH meter (Orion Star™, Thermo Electron Co., USA) was equipped with an Orion® 8102BN Ross combination electrode (Thermo Electron Co., USA) against two or three standard buffers. During field surveys, two pH buffer sets were used. The first set included three NIST (National Institute of Standards and Technology)-traceable buffers (pH = 4.01, 7.00, and 10.01 at 25.0 °C; Thermo Fisher Scientific Inc., USA), which were used during all surveys. The second set was used only during the June and November surveys, and included two carefully prepared solutions of 2-amino-2-hydroxy-1,3-propanediol (tris) and 2-aminopyridine, which are used by chemical oceanographers as pH_T buffers (Dickson et al., 2007). Based on parallel measurements in June and November using the two pH buffer sets, the pH_T data were lower than the NIST-traceable pH data by 0.143 ± 0.003 pH units (mean ± standard deviation, $n = 62$) in the study area (Fig. A1), which was comparable to Bohai Sea results (Zhai et al., 2012) and the commonly accepted value for this difference (Lewis and Wallace, 1998). Based on this result, we transferred the other NIST-traceable pH data to the pH_T scale, although the pH_T buffers were not used during those surveys. The overall uncertainty of the pH data set was estimated to be 0.01 pH units (Marion et al, 2011; Zhai et al., 2012).

Water samples for DIC and TAlk analyses were also collected aboard. They were unfiltered but allowed to settle before measurement. As recommended by Huang et al. (2012), they were stored in 60 mL borosilicate glass bottles (for DIC) and 140 mL high-density polyethylene bottles (for TAlk). They were mixed with 50 µL saturated $HgCl_2$ and sealed with screw caps and preserved at room temperature. DIC was measured by infrared detection following acid extraction of a 0.5 mL sample with a Kloehn® digital syringe pump, as described in Cai et al. (2004). TAlk was determined by Gran acidimetric titration on a 25 mL sample with another Kloehn® digital syringe pump, using the precision pH meter and an Orion® 8102BN Ross electrode for detection. During DIC and TAlk determinations, Certificated Reference Materials from A. G. Dickson's lab were used for quality assurance at a precision level of ± 2 µmol kg^{-1} (Cai et al., 2004; Dickson et al., 2007).

For chl *a* determination, water samples from 300 to 1000 mL were filtered on board, depending on the chl *a* concentration. Filters were folded and wrapped in aluminium foil, and stored in liquid nitrogen until analysis. After extraction by acetone, concentrations of chl *a* were measured using a TD-700 laboratory fluorometer (Turner Designs, USA) with excitation and emission wavelengths set at 430 and 670 nm, respectively (Parsons et al., 1984).

2.4 Calculation of other carbonate system parameters

The seawater fugacity of CO_2 (fCO_2), pH_T (in situ), and Ω_{arag} were calculated from DIC, TAlk, seawater temperature, and salinity using the calculation program CO2SYS.xls (Pelletier et al., 2011), which is an updated version of the original CO2SYS.EXE (Lewis and Wallace, 1998). For the January 2012 cruise, however, DIC data were not available due to sample loss. Therefore, the fCO_2, pH_T (in situ), Ω_{arag} and DIC values from this specific cruise were calculated based on pH_T (at 25 °C) and TAlk, using the same calculation program. The dissociation constants for carbonic acid were those determined by Millero et al. (2006), and the dissociation constant for the HSO_4^- ion was determined as per Dickson (1990). The K^*_{sp} values for aragonite were taken from Mucci (1983), and the Ca^{2+} concentrations were assumed to be proportional to salinity. By comparison with measured Ca^{2+} data for our June, August, and November cruises (Zhai, unpublished data), nearly all relative deviations of calculated Ca^{2+} values were at satisfactory levels (< 2 %; plots not reported).

All available information and measured and calculated data in the sampled bottom waters are presented in the Supplement for public reference. To further assess the quality of this data set, the calculated DIC (from field-measured pH at 25 °C and TAlk) versus measured DIC, calculated pH (from DIC and TAlk) versus field-measured pH, and Ω_{arag} values from DIC and TAlk versus those from field-measured pH (at 25 °C) and TAlk were compared (Fig. A2). For DIC and pH, most measured data and calculated results were consistent with each other at deviation levels of $\pm 15\,\mu mol\,kg^{-1}$ (DIC) and ±0.05 (pH). These deviation levels were reasonably higher than the precision of DIC determination ($\pm 2\,\mu mol\,kg^{-1}$) and the uncertainty of the measured pH data (±0.01 pH units). Furthermore, the two sets of Ω_{arag} values were mostly consistent with each other at a minor deviation level of ±0.1. Some Ω_{arag} values from DIC and TAlk were slightly higher than those from field-measured pH (at 25 °C) and TAlk by 0.1 to 0.2. These comparisons suggested that the measured data and calculated results of the carbonate system parameters were reliable.

3 Results

3.1 Environmental settings

The surveys covered four seasons fully. In January, a winter month, water temperature at deeper stations (water depth > 25 m, the same below) ranged between 3.19 °C and 6.74 °C (Fig. 3). Lower temperatures – between −1.45 °C and 0.64 °C – were also measured (Fig. 3g) at two northern stations (enclosed by the purple ellipse in Fig. 1). From late spring to late summer, sea surface temperature (SST) increased from 6.62−13.46 °C in May to 11.24−19.75 °C in June and to 19.22−24.83 °C in July–August (Fig. 3a–d, 3g), while the mean bottom-water temperature of deeper stations increased from 5.48 ± 1.23 °C in May and 6.95 ± 2.43 °C in June to 8.98 ± 3.21 °C in July and to 13.65 ± 4.92 °C in August (Fig. 4a). Therefore, it is evident that strong water column stratification occurred at most stations in the summer months (June to August) (Fig. 3b–d), except for a well-mixed station at the northeast corner during the June cruise. Summertime NYSCWM in bottom waters at a temperature of < 11 °C was identified in the study area (Fig. 5). From June to August, the area occupied by NYSCWM declined considerably (Fig. 5b–d), while the lowest bottom-water temperature increased from 3.84 °C in June to 4.21 °C in July and 5.07 °C in August (Fig. 3b–d). In October, despite the fact that surface waters had cooled to between 14.73 and 18.37 °C, water column stratification still persisted (Fig. 3e). In November, SST further declined to between 11.47 °C and 14.53 °C (Fig. 3f), while temperature-induced water column stratification started to disappear at the northern or western stations with bottom-water temperatures of > 11 °C (Fig. 5f). Note that in the two autumn months, another bottom cold water of < 11 °C was constructed in the southeastern part of the study area (Fig. 5e–f), presumably influenced by the adjacent SYS bottom waters (Chen, 2009).

Compared with the significant seasonal variation in bottom-water temperatures (from 5.48 ± 1.24 °C in May 2011 to 13.65 ± 4.92 °C in August 2011 at deeper stations), bottom-water salinity at the deeper stations only changed on average between 31.32 ± 0.60 in August 2011 and 31.89 ± 0.33 in May 2011 (Fig. 4a). However, bottom-water salinity at shallower stations in the southwestern part of the study area showed seasonal variations (Fig. 5a–f); in May and June, bottom-water salinity values were at relatively high levels (31.50 to 32.00; Fig. 5a–b), but showed relatively low levels (30.50 to 31.50) from July to November (Fig. 5c–f). This was roughly consistent with the seasonal variation of water discharge from the Yellow River (Fig. 2b). In 2011, both late June and late September showed peak water discharge ($\sim 3000\,m^3\,s^{-1}$) from the Yellow River. River discharge of $3.73 \times 10^9\,m^3$ over 18 days (24 June to 11 July) and $2.34 \times 10^9\,m^3$ over 14 days (17 to 30 September) enhanced the outflow of the relatively low-salinity Bohai Sea water along the southern coastline of the study area

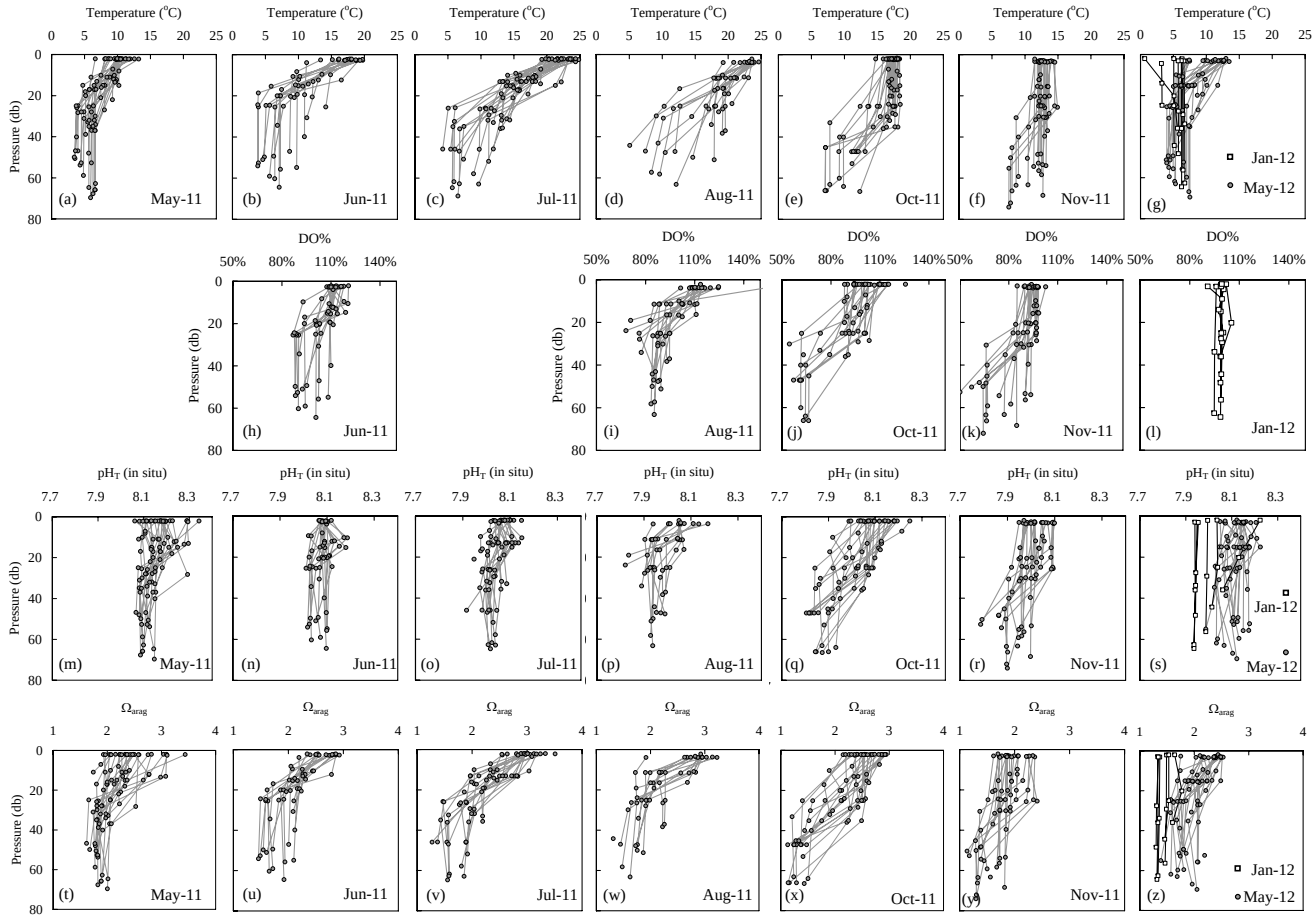

Fig. 3. Depth profiles of water temperature **(a–g)**, dissolved oxygen saturation **(h–l)**, pH$_T$ **(m–s)**, and carbonate saturation state of aragonite **(t–z)**.

(Fig. 5c–f). On seasonal or shorter time scales, this water was generally confined to the southwestern part of the study area (enclosed by the blue ellipse in Fig. 1), which was further evidenced by our temperature–salinity diagrams (Fig. 6a–h).

Sea surface DO% ranged between 85 % (in November) and 154 % (in August) (Fig. 3h–l). In subsurface waters, relatively high DO% (from 86 % to 112 %) was observed in both June and January (Fig. 3h, 3l). However, relatively low subsurface DO% values were observed in August (68 % to 95 %, Fig. 3i), October (54 % to 104 %, Fig. 3j), and November (51 % to 98 %, Fig. 3k). In January, DO% values ranged between 94 % and 105 % in water columns (Fig. 3l), indicating that winter DO was in equilibrium with the atmosphere. The high sea surface DO% values (from 110 % to 154 % in June, August, and October; Fig. 3h–j) were consistent with the high chl *a* and primary production levels in the study area (Gao and Li, 2009; Yang et al., 2009; Tan et al., 2011; He et al., 2013; Fig. 7). In November, however, the mixing of surface and oxygen-depleted subsurface waters led to undersaturated DO (DO% ranged from 85 % to 98 %) in sea surface waters (Fig. 3k).

As an indication of primary production levels, sea surface chl *a* data were also collected in May, July, and October 2011, and January 2012 (Fig. 7). They were measured at 0.75 to 8.17 $\mu g\,L^{-1}$ (average $1.96 \pm 1.42\,\mu g\,L^{-1}$) in May, 0.44 to 6.32 $\mu g\,L^{-1}$ (average $1.87 \pm 1.58\,\mu g\,L^{-1}$) in July, 0.81 to 10.97 $\mu g\,L^{-1}$ (average $3.29 \pm 2.70\,\mu g\,L^{-1}$) in October, and 0.33 to 2.81 $\mu g\,L^{-1}$ (average $1.06 \pm 1.01\,\mu g\,L^{-1}$) in January. These seasonal values were all comparable to or higher than those from the shelf of the subtropical East China Sea, where the sea surface chl *a* was determined at 0.26 to 2.09 $\mu g\,L^{-1}$ in December 1997 (winter), 0.15 to 1.85 $\mu g\,L^{-1}$ in March 1998 (early spring), 0.11 to 8.03 $\mu g\,L^{-1}$ in July 1998 (summer), and 0.28 to 2.75 $\mu g\,L^{-1}$ in October 1998 (autumn) (Gong et al., 2003). Earlier survey-based and satellite-based studies also revealed high chl *a* and primary production levels in the study area (e.g. Gao and Li, 2009; Yang et al., 2009; Tan et al., 2011; He et al., 2013).

Significantly, extremely high sea surface chl *a* values (4.12 to 6.32 $\mu g\,L^{-1}$ in July in the northern and southwestern parts, and 10.97 $\mu g\,L^{-1}$ in October in the northern part of the study area) (Fig. 7c) indicated very high primary production levels

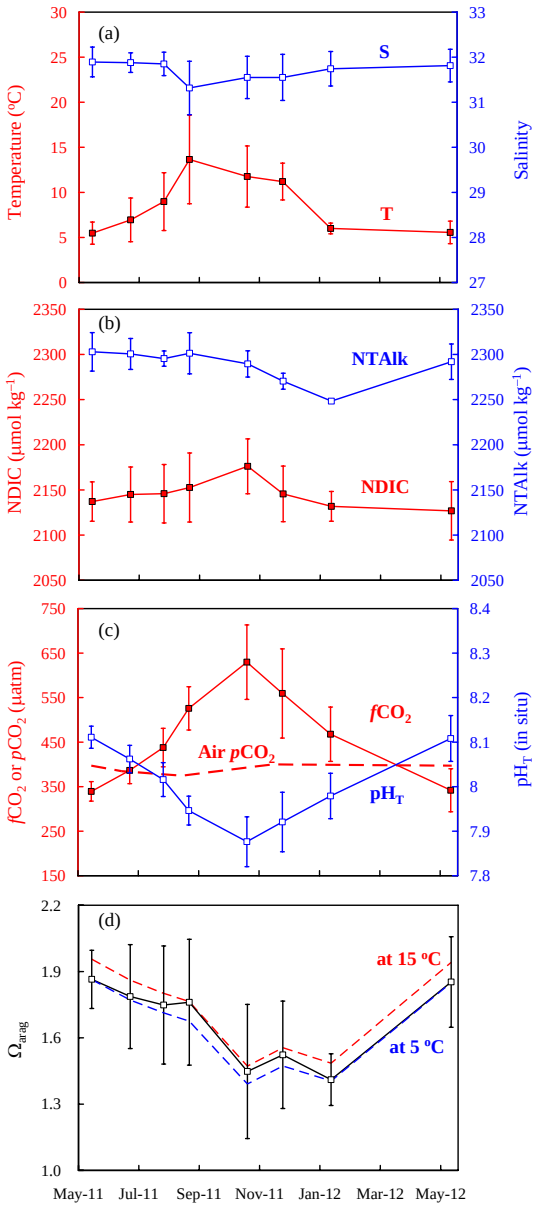

Fig. 4. Time series of averaged survey values of bottom-water temperature/salinity **(a)**, salinity-normalized total alkalinity (NTAlk)/dissolved inorganic carbon (NDIC) **(b)**, fugacity of CO_2 and pH_T **(c)**, and carbonate saturation state of aragonite **(d)** at deeper stations (water depth > 25 m). Error bars denote standard deviations. NTAlk and NDIC were calculated according to Eqs. (6)–(11) (Sect. 3.2). Dashed line in panel **(c)** shows monthly mean air pCO_2 (partial pressure of CO_2), i.e. air-equilibrated level of fCO_2 calculated from the flask analysis data of atmospheric CO_2 concentration at the adjacent Tae-ahn Peninsula (TAP) site (36°44′ N 126°08′ E), and corrected to survey-based barometric pressure at 10 m above the sea surface and 100 % humidity at sea surface temperature and salinity, following the procedure described in Zhai et al. (2009).

in the northern and southwestern areas in 2011. According to the marine environmental status bulletin released by the State Oceanic Administration of China, seven cases of red tide were recorded in 2011 in the northern part of the study area (State Oceanic Administration of China, 2012), which was generally consistent with the chl *a* results. This is detailed in the Supplement. These red tides probably produced large sinking fluxes of particulate organic matter, leading to bottom-water DO depletion and pH decline (Eq. (1)). The relationship between bottom-water DO depletion and pH decline shall be discussed in detail in Sect. 4.2.

3.2 TAlk and DIC and their water mixing behaviours

In the study area, TAlk ranged between 2073 μmol kg^{-1} (at a salinity of 28.34 in August) and 2346 μmol kg^{-1} (at a salinity of 31.47 in May 2011) (Fig. 6i–p), while DIC ranged between 1809 μmol kg^{-1} (at a salinity of 28.34 in August) and 2214 μmol kg^{-1} (at a salinity of 31.77 in October) (Fig. 6q–w). In the adjacent eastern Bohai Sea, however, relatively high TAlk – from 2222 μmol kg^{-1} (at a salinity of 30.56 in October) to 2447 μmol kg^{-1} (at a salinity of 29.16 in May 2012) – was obtained (Fig. 6i–p).

TAlk, a nearly conservative parameter, showed complicated water mixing behaviours in the study area. Ideally, three-endmember or even four-endmember mixing models were needed to fully describe the complicated water mixing behaviours of the water column TAlk under multiple influences of river discharge (from Yalu River), the outflow of Bohai Sea water, and the intrusion of SYS water (Fig. 1). Fortunately, most bottom-water TAlk versus salinity at deeper stations followed several simple two-endmember mixing lines (Fig. 6i–p). From May to October 2011, the simplified water mixing line was

$$\text{TAlk}\ (\mu\text{mol kg}^{-1}) = 61.745 \times \text{Salinity} + 320\ (\text{from May to October 2011}). \quad (2)$$

This is much higher than the water mixing line between nearby open ocean surface waters (TAlk = 2300 to 2310 μmol kg^{-1} at the salinity of 35) (Chen and Wang, 1999) and rainwater. During the late autumn and winter cruises, however, the bottom-water mixing lines at deeper stations shifted from Eq. (2) to Eq. (3) in November 2011 and Eq. (4) in January 2012 (Fig. 6n–o).

$$\text{TAlk}\ (\mu\text{mol kg}^{-1}) = 56.814 \times \text{Salinity} + 452\ (n = 19,\ r = 0.95,\ \text{in November 2011}) \quad (3)$$

$$\text{TAlk}\ (\mu\text{mol kg}^{-1}) = 45.404 \times \text{Salinity} + 795\ (n = 6,\ r = 0.99,\ \text{in January 2012}) \quad (4)$$

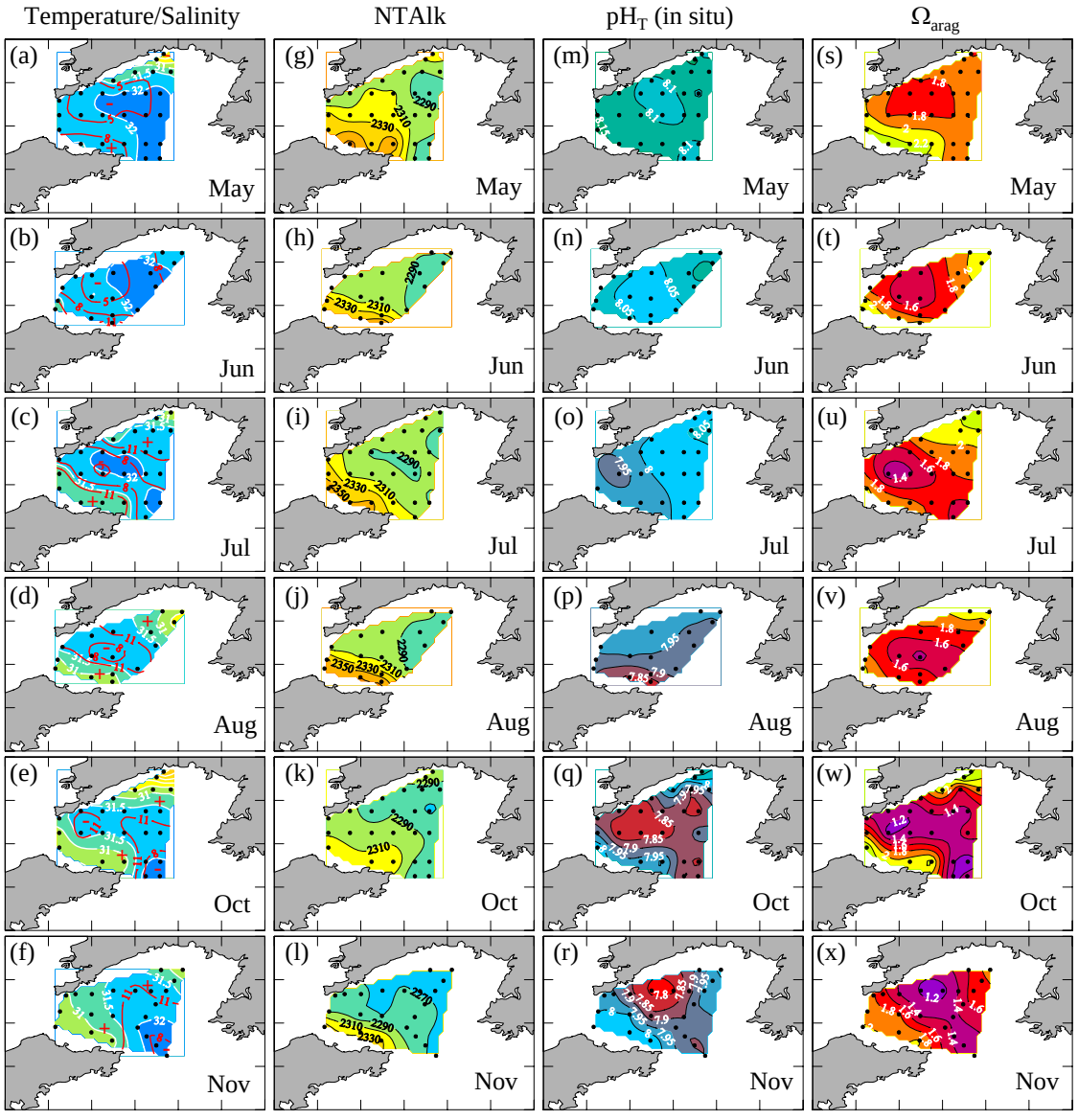

Fig. 5. Distributions of salinity/temperature **(a–f)**, salinity-normalized total alkalinity **(g–l)**, pH$_T$ **(m–r)**, and carbonate saturation state of aragonite **(s–x)** in bottom waters in May, June, July, August, October, and November 2011. Calculation of NTAlk is detailed in Sect. 3.2.

Therefore, the high-salinity endmember ($S = 32.1$) with high TAlk exhibited declining TAlk in the northeast monsoon seasons, which decreased by $\sim 20\,\mu mol\,kg^{-1}$ in November and $\sim 60\,\mu mol\,kg^{-1}$ in January compared with the usual value in the southwest monsoon seasons (TAlk = $2302\,\mu mol\,kg^{-1}$ at the salinity of 32.10 from May to October 2011) (Fig. 6i–o). These changes likely indicated the influences of the SYS water intrusion via YSWC in the northeast monsoon seasons (Fig. 1; Chen, 2009), as evidenced by the relatively high-salinity water intrusion ($S > 32.0$) at the bottom in the southeastern part of the study area in October and November (Fig. 5e–f). In addition, the TAlk values from 320 to 795 $\mu mol\,kg^{-1}$ at the extrapolated freshwater end were consistent with the low TAlk features of both the river plume from Yalu River and rainwater.

A typical nonconservative parameter, DIC is largely affected by both sea surface photosynthesis and subsurface respiration/remineralization. To characterize water mixing behaviours of water column DIC in the study area from May to October 2011, a two-endmember water mixing line was assumed (Eq. (5)).

$$\text{DIC}\ (\mu mol\,kg^{-1}) = 56.161 \times \text{Salinity} + 320\ (\text{from May to October 2011}) \quad (5)$$

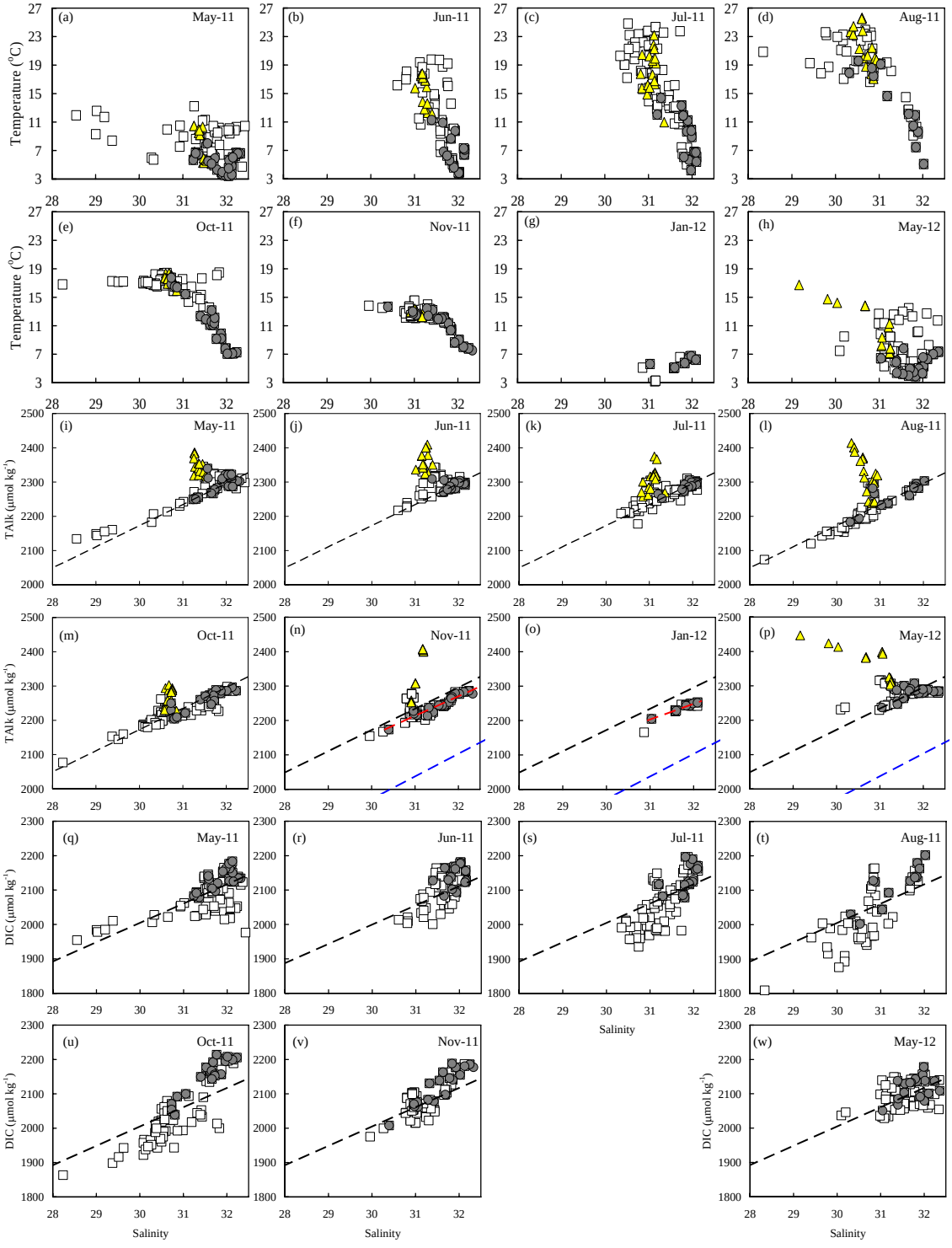

Fig. 6. Plots of temperature versus salinity **(a–h)**, total alkalinity versus salinity **(i–p)**, and dissolved inorganic carbon versus salinity **(q–w)** for each cruise. Open rectangles show all data in water columns in the study area, and grey circles represent bottom-water data in the study area. Yellow triangles denote the adjacent Bohai Sea data. Black dashed lines are TAlk (μmol kg^{-1}) = 61.745 × Salinity + 320 **(i–p)** and DIC (μmol kg^{-1}) = 56.161 × Salinity + 320 **(q–w)**, which are supposed as the bottom-water mixing lines from May to October. Red dashed lines in panels **(n–o)** are regression lines of total alkalinity in bottom waters, i.e. TAlk (μmol kg^{-1}) = 56.814 × Salinity + 452 in November, and TAlk (μmol kg^{-1}) = 45.404 × Salinity + 795 in January. Blue dashed lines in panels **(n–p)** are TAlk (μmol kg^{-1}) = 2305/35 × Salinity, which is the ideal mixing line between adjacent open ocean surface waters and rainwater (Chen and Wang, 1999; Lee et al., 2006).

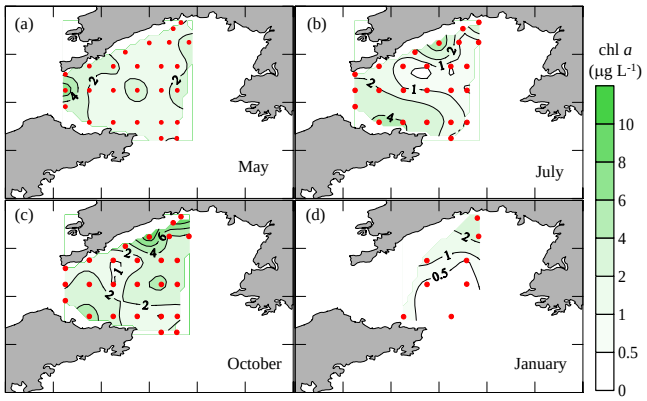

Fig. 7. Distributions of sea surface chlorophyll *a* concentrations in May, July, October 2011 and January 2012.

That is, a simple water mixing between an ideal freshwater endmember with DIC of 320 µmol kg^{-1} (equal to the above-mentioned freshwater endmember value of TAlk from May to October 2011) and a seawater endmember with DIC of 2123 µmol kg^{-1} at the salinity of 32.10. As shown in Fig. 6q–w, most DIC values in the water columns were lower than the predicted values due to sea surface biological uptake as indicated by relatively high chl *a* levels (Fig. 7). However, many bottom-water DIC values were higher than the predicted values (Fig. 6r–v), indicating respiration/remineralization-induced addition of DIC (Eq. (1)).

To eliminate the dilution and concentration effects of river discharge and precipitation and evaporation on the seawater carbonate system, we normalized bottom-water TAlk and DIC to a uniform salinity of 32. Following Friis et al. (2003), the salinity-normalized parameters (NTAlk and NDIC) were calculated as below.

In May, June, July, August, and October 2011, and May 2012,

$$\mathrm{NTAlk} = (\mathrm{TAlk} - 320\ \mu\mathrm{mol\ kg^{-1}}) \times 32 / \mathrm{Salinity} + 320\ \mu\mathrm{mol\ kg^{-1}}, \quad (6)$$

$$\mathrm{NDIC} = (\mathrm{DIC} - 320\ \mu\mathrm{mol\ kg^{-1}}) \times 32 / \mathrm{Salinity} + 320\ \mu\mathrm{mol\ kg^{-1}}. \quad (7)$$

In November 2011,

$$\mathrm{NTAlk} = (\mathrm{TAlk} - 452\ \mu\mathrm{mol\ kg^{-1}}) \times 32 / \mathrm{Salinity} + 452\ \mu\mathrm{mol\ kg^{-1}}, \quad (8)$$

$$\mathrm{NDIC} = (\mathrm{DIC} - 452\ \mu\mathrm{mol\ kg^{-1}}) \times 32 / \mathrm{Salinity} + 452\ \mu\mathrm{mol\ kg^{-1}}. \quad (9)$$

In January 2012,

$$\mathrm{NTAlk} = (\mathrm{TAlk} - 795\ \mu\mathrm{mol\ kg^{-1}}) \times 32 / \mathrm{Salinity} + 795\ \mu\mathrm{mol\ kg^{-1}}, \quad (10)$$

$$\mathrm{NDIC} = (\mathrm{DIC} - 795\ \mu\mathrm{mol\ kg^{-1}}) \times 32 / \mathrm{Salinity} + 795\ \mu\mathrm{mol\ kg^{-1}}. \quad (11)$$

In the southwestern part of the study area, a tongue-like region with a relatively high NTAlk from 2310 to 2370 µmol kg^{-1} was identified in bottom waters (Fig. 5g–l). This region was rather shallow (water depth mostly < 25 m) and likely influenced by the outflow of the relatively low-salinity Bohai Sea water. Focusing on the deeper stations, 75 % of the bottom-water NTAlk values were in a compact range of 2290 ± 25 µmol kg^{-1} (Fig. 8). This specific value was slightly lower than the cruise mean bottom-water NTAlk values of deeper stations from May to August 2011 (between 2295 ± 9 µmol kg^{-1} in July and 2303 ± 22 µmol kg^{-1} in May), but quite consistent with the cruise mean bottom-water NTAlk values of deeper stations in October 2011 (2290 ± 15 µmol kg^{-1}) and May 2012 (2292 ± 20 µmol kg^{-1}) (Fig. 4b). During the November and January cruises, the mean bottom-water NTAlk values were only 2270 ± 9 µmol kg^{-1} in November and 2248 ± 2 µmol kg^{-1} in January (Fig. 4b), likely reflecting the influence of the SYS water intrusion, as mentioned above.

The cruise mean bottom-water NDIC values of deeper stations increased from 2137 ± 22 µmol kg^{-1} in May 2011 to 2176 ± 31 µmol kg^{-1} in October 2011, and then gradually declined to 2127 ± 33 µmol kg^{-1} in May 2012 (Fig. 4b). Therefore, a baseline value of NDIC (2130 µmol kg^{-1}) was obtained for this study, which was roughly free from the modulation of sea surface photosynthesis and subsurface respiration/remineralization. In August, October and November, most bottom-water NDIC data at the deeper stations were higher than the baseline value, especially at the salinity range from 31.63 to 32.25 (Fig. 8), which was possibly due to the community respiration- and/or aerobic remineralization-induced addition of DIC in bottom waters (see Sect. 4.2).

3.3 Seasonal variations of bottom-water fCO_2, pH_T and Ω_{arag}

Figure 4c shows seasonal variations of bottom-water fCO_2 and pH_T at the deeper stations. On average, bottom-water fCO_2 increased from CO_2-undersaturated 339 ± 22 µatm in May 2011 and 342 ± 49 µatm in May 2012 to nearly air-equilibrated 387 ± 30 µatm in June to CO_2-supersaturated 438 ± 4 µatm in July, 526 ± 49 µatm in August, and 630 ± 84 µatm in October. In November and January, bottom-water fCO_2 declined to 560 ± 100 µatm and 468 ± 61 µatm, respectively. Overall, bottom water pH_T mirrored fCO_2 (Fig. 4c), which declined from relatively high levels of 8.11 ± 0.03 in May 2011 and 8.11 ± 0.06 in May 2012 to 8.06 ± 0.04 in June, 8.02 ± 0.04 in July, and 7.94 ± 0.04 in August, reaching the lowest value of 7.88 ± 0.06 in October. In November and January,

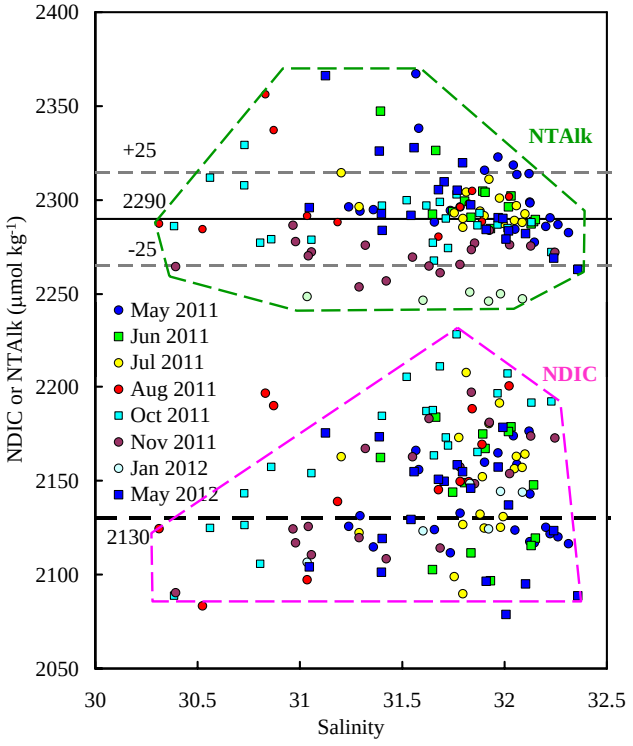

Fig. 8. Salinity-normalized total alkalinity (NTAlk) and salinity-normalized dissolved inorganic carbon (NDIC) versus salinity at deeper stations (water depth > 25 m). Calculations of NTAlk and NDIC are detailed in Sect. 3.2. Grey dashed lines show a range of $\pm 25\,\mu mol\,kg^{-1}$, while the dark dashed line shows the assumed baseline value of NDIC in this study.

bottom-water pH_T increased to 7.92 ± 0.07 and 7.98 ± 0.06, respectively.

Seasonal variation in bottom-water Ω_{arag} (Fig. 4d) was more complicated than pH_T and fCO_2. From spring to summer, bottom-water Ω_{arag} declined slightly from 1.86 ± 0.14 in May 2011 and 1.85 ± 0.21 in May 2012 to 1.79 ± 0.24 in June, 1.75 ± 0.27 in July, and 1.76 ± 0.29 in August. In autumn and early winter, cruise mean bottom-water Ω_{arag} was 1.45 ± 0.31 in October, 1.52 ± 0.25 in November, and 1.41 ± 0.12 in January.

Figure 5 also shows seasonal variations in bottom-water pH_T and Ω_{arag} distributions. The low pH_T area ($pH_T < 7.90$) and low Ω_{arag} area ($\Omega_{arag} < 1.40$) reached peaks in October (Fig. 5). In this month of maximum acidification, low pH_T values of 7.81 to 7.90 were detected at 15 stations, covering the main body of the study area (Fig. 5q). In these stations, bottom-water pH_T declined by 0.17 to 0.30 units from May to October, demonstrating significant increases in bottom-water total-hydrogen-ion concentrations by 48 % to 100 % over the six months. In November, low pH_T values (7.79 to 7.90) were detected at six northern stations and two south-eastern stations (Fig. 5r). Low Ω_{arag} values (1.13 to 1.40) were detected at ten stations in October and seven stations in November (Fig. 5w–x), while such low Ω_{arag} values were rarely observed in spring and summer (Fig. 5s–v).

Vertical profiles suggested that most pH_T values of less than 7.90 and Ω_{arag} values of less than 1.40 were observed from July to October and were confined to subsurface waters (below 25 m depth) due to stratification (Fig. 3). They became higher in November and January, when bottom waters were mixed with sea surface waters (Fig. 3r–s, 3y–z).

In the previously mentioned tongue-like region in the southwestern part of the study area, bottom-water Ω_{arag} was at relatively high levels (1.80 to 2.40; Fig. 5s–x), although low pH_T values (from 7.82 to 7.90) were also detected in August (Fig. 5p). Salinity distributions suggested that both the highest fCO_2 values and lowest pH_T and Ω_{arag} values were associated with relatively high salinity (31.63 to 32.25) in bottom waters (Fig. 9), where significant DO depletion was observed (Fig. 10).

3.4 Subsurface community respiration in summer and autumn

Variations in bottom-water DO following changes in salinity are shown in Fig. 10. In June, the average bottom-water DO was $291 \pm 12\,\mu mol\text{-}O_2\,kg^{-1}$ ($n = 13$, salinity range 31.65 to 32.15, DO% range 88 % to 110 %), which was similar to the air-equilibrated DO in winter (286 to 311 $\mu mol\text{-}O_2\,kg^{-1}$). In August, a rather uniform bottom-water DO level of $243 \pm 7\,\mu mol\text{-}O_2\,kg^{-1}$ ($n = 5$, DO% range 83 % to 89 %) corresponded to a narrow salinity range (from 31.78 to 31.89; Fig. 10). In October, three bottom-water DO clusters were identified at different salinity ranges (Fig. 10). Of these clusters, one with relatively high salinity (32.13 to 32.23) exhibited an average DO of $193 \pm 5\,\mu mol\text{-}O_2\,kg^{-1}$ (including two DO values of 188 and 198 $\mu mol\text{-}O_2\,kg^{-1}$, with a DO% of 63 % and 66 %, respectively). The second cluster had DO values of 176 and 181 $\mu mol\text{-}O_2\,kg^{-1}$ (average 178 $\mu mol\text{-}O_2\,kg^{-1}$, with DO% of 61 % and 64 %, respectively) and salinity values of 31.87 and 31.88. The third cluster, with relatively a low salinity (from 31.65 to 31.73) had an average DO of $162 \pm 7\,\mu mol\text{-}O_2\,kg^{-1}$ ($n = 4$; DO% range 57 % to 62 %). Since water column stratification was intensified from June to October (Fig. 3), replenishing of oxygen via vertical mixing was possibly negligible during these months. Therefore, the apparent DO depletion rate can be regarded as a rough estimate of the subsurface community respiration rate.

Based on Fig. 10, the bottom-water community respiration rates at different salinity ranges were estimated in Table 2. All results were in the narrow range of 0.80 to 1.08 $\mu mol\text{-}O_2\,kg^{-1}\,d^{-1}$ (overall salinity range from 31.63 to 32.25), suggesting relatively low community respiration rates in the high-salinity bottom waters from summer to autumn, as compared to the earlier values of 2.00 to 2.80 $\mu mol\text{-}O_2\,kg^{-1}\,d^{-1}$ observed in summer oxygen-depleted bottom waters in the adjacent Bohai Sea (Zhai et al., 2012).

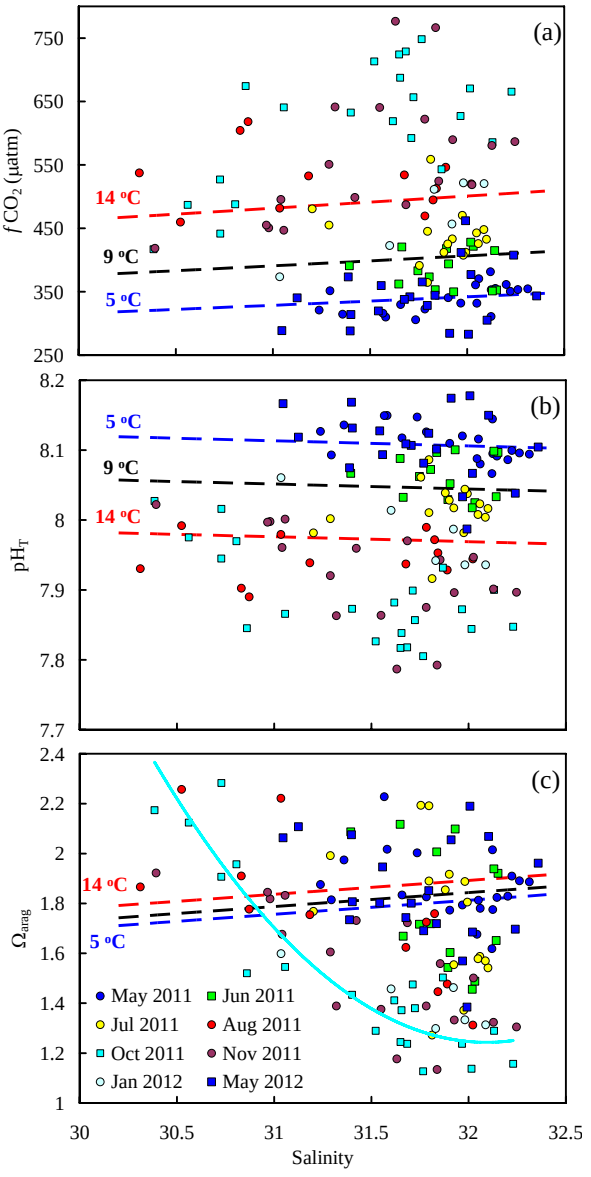

Fig. 9. Fugacity of CO_2 versus salinity **(a)**, pH_T versus salinity **(b)**, carbonate saturation state of aragonite versus salinity **(c)** in bottom water at deeper stations (water depth > 25 m). Dashed lines are conservative mixing lines at 5 °C (blue), 9 °C (black), and 14 °C (red), based on bottom-water mixing lines of TAlk and DIC from May to October (Fig. 6), while the unbroken turquoise line in panel **(c)** shows the best-fitted conic for October data.

At the relatively low salinity range of 30.80 to 31.40, fairly low bottom-water DO values of 138 to 168 μmol-O_2 kg^{-1} (DO% range 54 % to 63 %) were also observed in October and November (Fig. 10), suggesting community respiration. Unfortunately, the rate within this salinity range was not calculable due to data limitation and potential water disturbance.

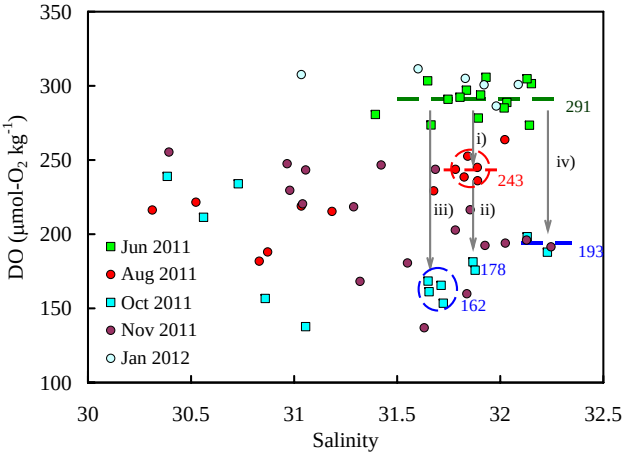

Fig. 10. Bottom water dissolved oxygen concentration versus salinity at deeper stations (water depth > 25 m).

4 Discussion

4.1 Effects of temperature

Prior to discussion on biogeochemical controls, the effects of temperature on fCO_2 (Takahashi et al., 1993), pH (Gieskes, 1969), and Ω_{arag} must be delineated and put into perspective. Figure 9 shows that a temperature increase from 5 °C to 14 °C led to a seawater fCO_2 increase of 155 ± 8 μatm (Fig. 9a) and a pH drop of ~0.137 units (Fig. 9b). This is because increasing temperature added a greater proportion of free CO_2 than that of CO_3^{2-} in water at a given salinity, TAlk, and pressure. Based on the seasonal increase in bottom-water temperature from May to August (5.48 ± 1.23 °C in May 2011, 8.98 ± 3.21 °C in July, and 13.65 ± 4.92 °C in August, Fig. 4a), we roughly predicted bottom-water fCO_2 and pH_T in May, July, and August (Fig. 9a, 9b).

However, the temperature-based prediction was not verified by our autumn data. From late summer (August) to autumn (October and November), although bottom temperature declined by ~2 °C (Fig. 4a), fCO_2 increased from 526 ± 49 μatm (August) to 630 ± 84 μatm (October) and 559 ± 101 μatm (November) (Fig. 4c), and pH_T decreased from 7.95 ± 0.04 (August) to 7.88 ± 0.06 (October) and 7.92 ± 0.07 (November) (Fig. 4c). The bottom-water fCO_2 increase and pH decline from late summer to autumn were both caused by local community respiration and/or aerobic remineralization, which induced an addition of DIC in bottom waters (see Sect. 4.2).

From late autumn to winter to early spring, temperature also had major effects on the bottom-water fCO_2 decline. As indicated by Fig. 4a, the average bottom-water temperature decreased by 5.20 °C from November to January (11.20 °C minus 6.00 °C). According to the approximate temperature coefficient of fCO_2 (4.23 % $°C^{-1}$) (Takahashi et al., 1993), this temperature decline could solely

Table 2. Calculation of bottom-water apparent dissolved oxygen (DO) depletion rates at deeper stations (water depth > 25 m). See Fig. 10 for details.

Serial number	Salinity	Duration	DO changes (μmol-O_2 kg^{-1})	Apparent DO depletion rate (μmol-O_2 kg^{-1} d^{-1})
(1)	between 31.78 and 31.89	June to August (60 d)	291 – 243 = 48	0.80
(2)	between 31.78 and 31.89	August to October (60 d)	243 – 178 = 65	1.08
(3)	between 31.63 and 31.72	June to October (120 d)	291 – 162 = 129	1.08
(4)	between 32.13 and 32.25	June to October (120 d)	291 – 193 = 98	0.82

account for the bottom-water fCO_2 drop of $\sim$ 100 µatm (average 560 µatm in November versus 467 µatm in January, Fig. 4c). In the northeast monsoon season, supposing the initially CO_2-equilibrated YSWC water quickly cooled from 9 °C to 5 °C and then submerged in the study area, the lower temperature could lead to a fCO_2 drop of $\sim$ 17 % or 68 µatm, which may explain the CO_2-undersaturated bottom waters observed in May (average $\sim$ 340 µatm, Fig. 4c).

In contrast with its major effects on fCO_2 and pH, temperature had only minor effects on Ω_{arag} (Figs. 4d, 9c). If bottom-water Ω_{arag} was calculated for a temperature of 5 °C or 15 °C instead of the in situ temperature, the changes in Ω_{arag} would only be −3 % or 5 % (Fig. 4d).

4.2 Controlling effects of community respiration on subsurface pH and Ω_{arag} declines from summer to autumn

To reveal the influences of community respiration and/or aerobic remineralization on carbonate system dynamics in subsurface waters, the bottom-water DIC, TAlk, pH, and Ω_{arag} data in the narrow salinity range of 31.63 to 32.25 were plotted against DO (Fig. 11). Field-measured pH_T (at 25 °C) were used to eliminate the influence of temperature on pH. To quantify the respiration-derived changes, relevant Redfield lines based on Eq. (1) were also plotted. As shown in Fig. 11, the plots of the four carbonate system parameters versus DO in relatively high salinity (31.63 to 32.25) bottom waters in June, August, October, and November satisfactorily followed the Redfield lines, suggesting controlling effects of community respiration and/or aerobic remineralization on pH and Ω_{arag} declines in these waters from summer to autumn.

From August to October, changes in bottom-water DIC/TAlk and thereby bottom-water fCO_2/pH_T/Ω_{arag} at the deeper stations were modelled based on Eq. (1) and the lower limit of the community respiration rate (0.80 µmol-O_2 kg^{-1} d^{-1}). During simulation, initial NTAlk and NDIC were set to the August values of 2300 µmol kg^{-1} and 2150 µmol kg^{-1}, respectively (Fig. 4b), while salinity and temperature were replaced by constant values of 31.50 and 12.50 °C, respectively (Fig. 4a). The simulation results (plot not reported) suggested that community respiration and/or aerobic remineralization led to a bottom-water fCO_2 increase from 500 µatm in late August to 670 µatm in late October, a pH_T decrease from 7.97 to 7.85, and an Ω_{arag} decline from 1.76 to 1.38. All latter values were close to the field-based data in October (fCO_2 630 ± 84 µatm, pH_T 7.88 ± 0.06, and Ω_{arag} 1.45 ± 0.31 at deeper stations, Fig. 4). On average, however, the field-based Ω_{arag} decline from August to October (1.76−1.45 = 0.31, Fig. 4d) was equal to only 82 % of the predicted Ω_{arag} decline value (1.76−1.38 = 0.38), suggesting other processes counteracting the seasonally and locally intensified acidification. This issue will be discussed in Sect. 4.3.

4.3 Potential precipitation/dissolution of $CaCO_3$ and influences of water mixing

Bottom water NTAlk, pH_T (at 25 °C) and Ω_{arag} versus NDIC showed diverse patterns at a relatively high salinity range (31.63 to 32.25) (Fig. 12) and a relatively low salinity range (30.31 to 31.59) (Fig. 13). To further discuss the impacts of biogeochemical processes (including water mixing) on bottom-water pH and Ω_{arag}, several stoichiometric relationships were modelled based on ideal changes of DIC and TAlk associated with community respiration and aerobic remineralization, calcification, and $CaCO_3$ dissolution in different waters (Figs. 12, 13).

4.3.1 Relatively high salinity bottom waters

In the relatively high salinity (31.63 to 32.25) bottom waters, pH_T / Ω_{arag} versus NDIC plots suggested that three biogeochemical processes affected carbonate system dynamics (Fig. 12). In addition to the major effects of community respiration and/or aerobic remineralization, signals of precipitation and dissolution of $CaCO_3$ were revealed. As mentioned above, the study area is abundant in bivalve molluscs that inhabit bottom waters. Although no direct measurement was made, bottom-water calcification was possible in spring due to the relatively high Ω_{arag} of 1.69 to 2.19 (Fig. 5s). In summer and autumn, however, bottom-water Ω_{arag} declined to between 1.13 and 1.40 at many stations (Fig. 5u–x), where $CaCO_3$ biominerals in native-born calcic shells may have undergone dissolution (Xu et al., 2013).

As represented with chemical reaction equations, calcification lowers TAlk by two equivalents and DIC by one mole

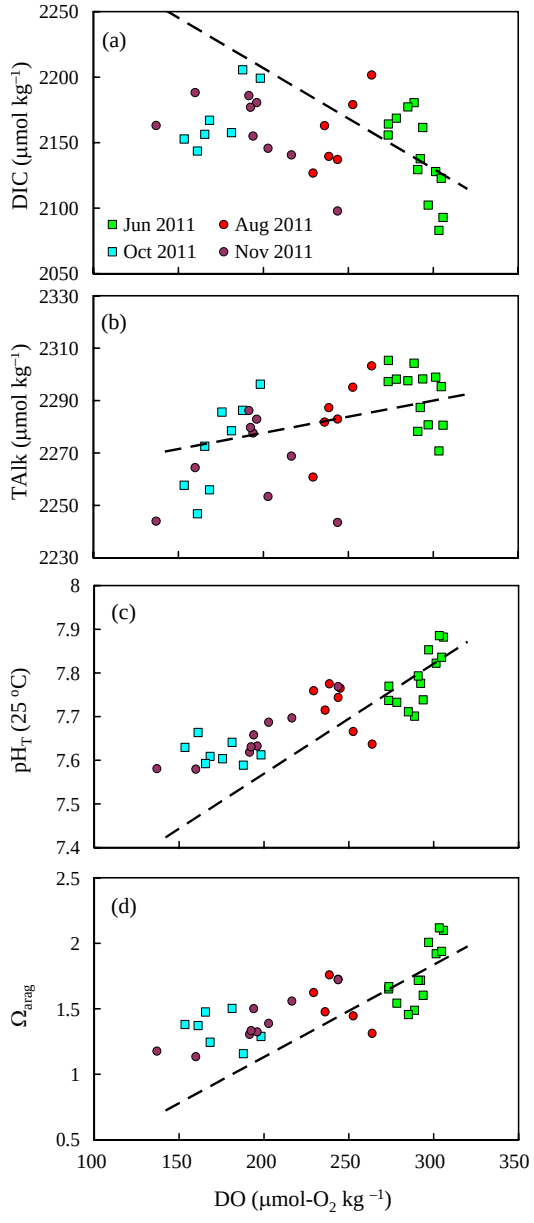

Fig. 11. Bottom water TAlk/DIC and pH_T/Ω_{arag} versus DO at the salinity range of 31.63 to 32.25. Dashed lines are modelled relationships based on the Redfield equation. To eliminate temperature effects on pH, field-measured pH_T (at 25 °C) instead of pH_T (in situ) were used in panels **(c)**.

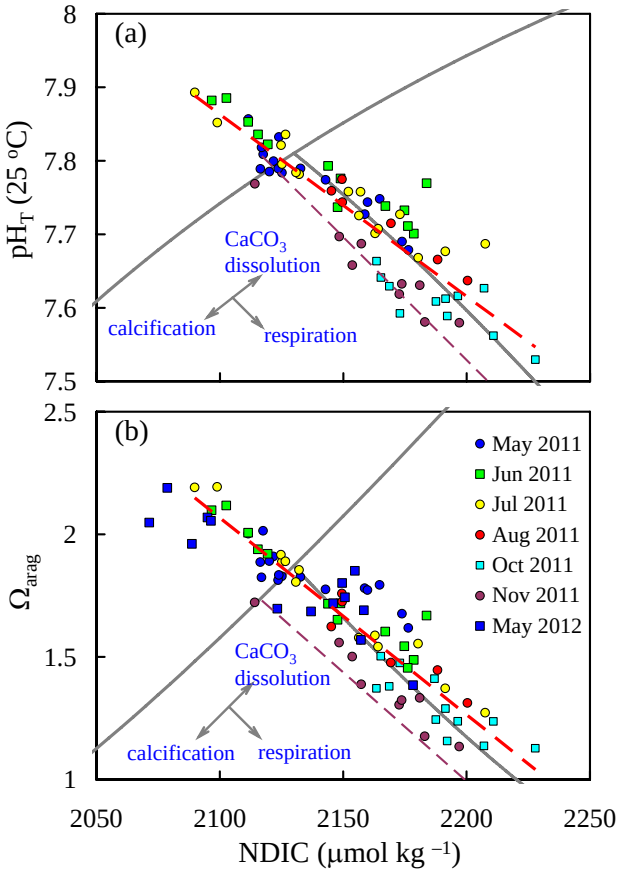

Fig. 12. Bottom water pH_T/Ω_{arag} versus salinity-normalized DIC (NDIC) at the salinity range of 31.63 to 32.25. Calculation of NDIC is detailed in section 3.2. To eliminate temperature effects on pH, field-measured pH_T at 25 °C instead of pH_T (in situ) were used. Usual relationships derived from ideal changes of pH_T/Ω_{arag} versus NDIC in aerobic respiration, $CaCO_3$ dissolution, and calcification are delineated by grey lines. Dashed red lines are best-fitted regression lines of all data. Dashed violaceous lines are ideal changes of pH_T/Ω_{arag} versus NDIC in respiration based on carbonate system obtained during our November cruise.

for every mole of $CaCO_3$ precipitated (Eqs. (12) and (13)). In addition, $CaCO_3$ dissolution raises TAlk by two equivalents for every mole of DIC increase (Eq. (14)). As indicated by the arrows in Fig. 12, the precipitation of $CaCO_3$ lowered Ω_{arag} and pH due to the decline in CO_3^{2-} ion concentration (Eq. (12)) or the increase in free CO_2 concentration (Eq. (13)), and vice versa for $CaCO_3$ dissolution (Eq. (14)).

$$Ca^{2+} + CO_3^{2-} \rightarrow CaCO_3 \quad (12)$$

$$Ca^{2+} + 2HCO_3^- \rightarrow CaCO_3 + CO_2 + H_2O \quad (13)$$

$$CaCO_3 + CO_2 + H_2O \rightarrow Ca^{2+} + 2HCO_3^- \quad (14)$$

At the relatively low NDIC range of 2070 to 2137 μmol kg^{-1} (with relatively high Ω_{arag} of 1.69 to 2.19) during the two spring cruises, several bottom-water Ω_{arag} values were 6 % to 11 % lower, and several bottom-water pH_T (at 25 °C) values were 0.02 to 0.05 units lower than those predicted by the Redfield relationship (Fig. 12). Both were influenced by possible calcification. However, most Ω_{arag} and pH values with relatively high NDIC values of 2143 to 2228 μmol kg^{-1}

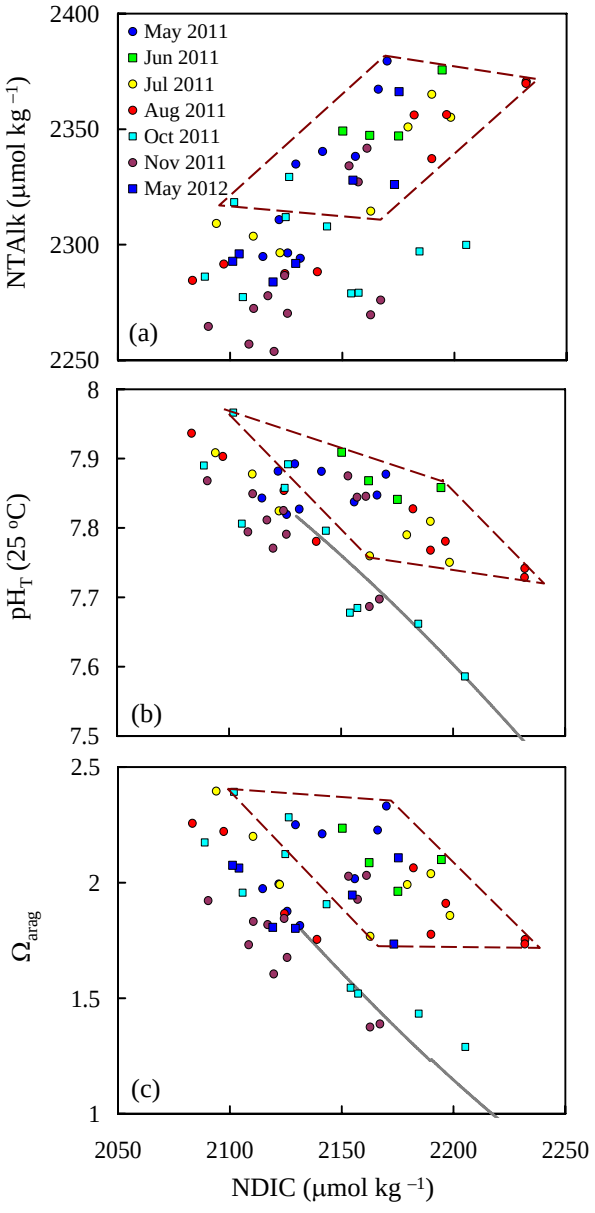

Fig. 13. Bottom water NTAlk/pH_T/Ω_{arag} versus NDIC at the salinity range of 30.31 to 31.59. Calculations of NTAlk and NDIC are detailed in Sect. 3.2. To eliminate temperature effects on pH, field-measured pH_T at 25 °C instead of pH_T (in situ) were used. Data points enclosed by brown quadrangles are from the southwestern region of the study area (enclosed by the blue ellipse in Fig. 1). Grey lines show the Redfield relationship outside the southwestern region of the study area.

ranged between the two modelled lines of aerobic respiration and $CaCO_3$ dissolution. In July, August, and October, several bottom-water Ω_{arag} values were ∼ 13 % higher and several bottom-water pH_T (at 25 °C) values were ∼ 0.06 units higher than those predicted by the Redfield relationship (Fig. 12). These differences may result from CO_2-consuming $CaCO_3$ dissolution (Eq. (14)). In November, however, NTAlk declined by ∼ 20 μmol kg^{-1} compared with the specific value (2290 μmol kg^{-1}) in southwest monsoon seasons (Fig. 8), leading to a downward shift in Redfield lines (Fig. 12). Therefore, the November bottom-water data also suggested $CaCO_3$ dissolution as discussed above.

In summary, the carbonate system parameters versus DIC plots suggested that high-salinity bottom waters in the study area may undergo both precipitation (in spring) and dissolution (in summer and autumn) of $CaCO_3$. The latter process may be utilized to combat locally intensified acidification and to mitigate its impacts on valuable bivalve molluscs (Green et al., 2009; Kelly et al., 2011).

4.3.2 Relatively low-salinity bottom waters

In the relatively low-salinity (30.31 to 31.59) bottom waters, data points of NTAlk versus NDIC were divided into two clusters (Fig. 13a), corresponding to the above-mentioned two low-salinity regions (Fig. 5a–f). Very high NTAlk values (from 2315 to 2379 μmol kg^{-1}) were observed in the southwestern region of the study area, which was likely influenced by the outflow of Bohai Sea water (enclosed by the blue ellipse in Fig. 1). Other NTAlk values were obtained in the northeastern study area under the influence of water discharge from Yalu River (Fig. 1). Accordingly, Ω_{arag} and pH_T (at 25 °C) versus NDIC showed two different relationships (Fig. 13b–c). In the area under the possible influence of the outflow of Bohai Sea water, the bottom-water Ω_{arag} was at relatively high levels of 1.73 to 2.39 (Fig. 13c). Similarly, the bottom-water pH_T (at 25 °C) in the southwestern region was 0.04 to 0.24 higher than the Redfield prediction values in another low-salinity region near the Yalu River estuary (Fig. 13b). Therefore, the outflow of Bohai Sea water could counteract the long-term reduction of subsurface Ω_{arag} in the study area if mixed with NYS bottom waters in late autumn and winter (Fig. 3). This issue needs further investigation.

4.4 Air–sea re-equilibration of CO_2-rich waters in winter

From late November to January, water cooling and the strong northeast monsoon destratified the water column (Fig. 3f–g), leading to a DO recovery by January (Fig. 3l). However, both pH and Ω_{arag} were still at low levels in this winter month (Fig. 3s, 3z), mainly due to the relatively high fCO_2 value of 468 ± 61 μatm in January (Fig. 4c). This is because air–sea re-equilibration of CO_2 is slower than DO due to the chemical buffering capacity of the marine carbonate system (e.g. DeGrandpre et al., 1997; Zeebe and Wolf-Gladrow, 2001; Zhai et al., 2009). Therefore, we cannot directly link DO change to DIC change during air–sea exchange. To resolve this issue, we intend to discuss the air–sea equilibration time

(τ). Following Zeebe and Wolf-Gladrow (2001),

$$\delta[O_2]/\delta t = k/d_{ML} \times ([O_2]_{equ} - [O_2]), \quad (15)$$

$$\delta DIC/\delta t = (\delta DIC/\delta[CO_2]) \times (\delta[CO_2]/\delta t), \quad (16)$$

$$\delta DIC/\delta t = k/d_{ML} \times ([CO_2]_{equ} - [CO_2]), \quad (17)$$

where prefix δ is the differential change, t is the time, k is the gas transfer velocity, d_{ML} is the mixed layer depth (75 m in winter), subscript equ is the air-equilibrated value. Therefore,

$$\tau(O_2) = ([O_2]_{equ} - [O_2])/(\delta[O_2]/\delta t) = d_{ML}/k, \quad (18)$$

$$\begin{aligned}\tau(CO_2) &= ([CO_2]_{equ} - [CO_2])/(\delta[CO_2]/\delta t) \\ &= d_{ML}/k \times (\delta DIC/\delta[CO_2]) \\ &= d_{ML}/k \times (DIC/[CO_2]/RF),\end{aligned} \quad (19)$$

where RF is the Revelle factor ($\sim$ 15 in acidified bottom waters). An eloquent definition of RF refers to Sundquist et al. (1979). To determine gas transfer velocity, the revised equation of Wanninkhof (1992) by Sweeney et al. (2007) was used, that is,

$$k = 0.27 \times u_{10}^2 \times (Sc/660)^{-0.5}, \quad (20)$$

where k is the gas transfer velocity (unit: cm h^{-1}), u_{10} is the wind speed at 10 m height, and Sc is the Schmidt number in seawater, calculated from temperature using a equation recommended by Wanninkhof (1992). During calculation, temperature and salinity were set to 6 °C and 32, respectively, while u_{10} was replaced by a constant value of 10 m s^{-1}.

The regional gas transfer velocities in winter was 4.39 m d^{-1}, which is reasonable and slightly higher than the global mean gas transfer velocity value (3.50 ± 1.12 m d^{-1}) derived from radiocarbon measurements (Sweeney et al., 2007). The $\tau(O_2)$ value was then determined to be 75/4.39 = 17 d. According to Zeebe and Wolf-Gladrow (2001), this $\tau(O_2)$ value meant that ($[O_2]_{equ}$ − $[O_2]$) declined, in the time span of 17 days, to 37 % of its initial value when water column stratification disappeared. This time scale was consistent with the bottom-water DO changes from October to November to January (Fig. 3j–l). However, bottom-water $\tau(CO_2)$ in the study area was $75/4.39 \times (2155/23.6/15) =$ 104 d in November and $75/4.39 \times (2120/24.0/15) = 100$ d in January. Both were 4.5 times longer than $\tau(O_2)$. The fCO_2 data from November 2011 to May 2012 (Fig. 4c) also suggested that a time span of nearly half a year, i.e. twice the $\tau(CO_2)$ value, was needed in order to fully ventilate the supersaturated CO_2 from water columns.

5 Summary and implications

We investigated the dynamics of subsurface pH and Ω_{arag} between May 2011 and May 2012 on the Chinese side of the North Yellow Sea. The results indicated that local community respiration and aerobic remineralization led to seasonal drops in subsurface pH and Ω_{arag}. Low pH_T values of 7.79 to 7.90 and low Ω_{arag} values of 1.13 to 1.40 dominated subsurface waters in October and November. In these waters, carbonate biominerals in calcic shells and skeletons may begin to dissolve.

In the broader context, increasing atmospheric CO_2 concentration (WMO/GAW, 2012) has induced sea surface carbonic acid levels to rise (Lenton et al., 2012), pH to decline (Caldeira and Wickett, 2003; Orr et al., 2005; Byrne et al., 2010), and carbonate ions to be titrated (Sabine et al., 2004; Turley and Gattuso, 2012), leading to declines in sea surface carbonate saturation state (Feely et al., 2012). These ocean acidification processes have been recognized as general CO_2 problems on the global scale (Doney et al., 2009). However, coastal oceans are more vulnerable to its impacts due to the combined stresses of complex oceanographic processes and increasing human activities (e.g. Thomas et al., 2007; Feely et al., 2008, 2010; Taguchi and Fujiwara, 2010; Cai et al., 2011; Kelly et al., 2011; Gruber et al., 2012; Sunda and Cai, 2012; Zhai et al., 2012; Chou et al., 2013; Duarte et al., 2013). This study clearly showed that this was also the case in the North Yellow Sea. The high-quality carbonate system data set will assist future predictions of marine environment changes in this important marginal sea under the context of ocean acidification.

In the China seas, several qualified carbonate system studies have shown that ocean acidification currently plays a minor role in lowering the $CaCO_3$ saturation state in the northern South China Sea and East China Sea shelves, where the lowest surface and bottom-water Ω_{arag} values were previously ascertained to be 1.70 to 2.00 (Cao et al., 2011; Chou et al., 2013). In the Bohai Sea, a summertime pH decline event has been reported (Zhai et al., 2012). However, the lowest bottom-water Ω_{arag} value was 1.69 in the bottom oxygen-depleted waters in the Bohai Sea in August 2011 (Zhai, unpublished data). The only $CaCO_3$-undersaturated case reported along the Chinese coastal zone is in the upstream region of the Pearl River Estuary, where $CaCO_3$ saturation for calcite was calculated to be 0.3 to 1.0 when salinity is on the range of 1 to 16 (Dai et al., 2006). Therefore, the NYS may represent one of the systems in the China seas most vulnerable to the potentially negative effects of ocean acidification. So far, however, it is not clear how marine organisms and ecosystems are affected by locally intensified acidification (e.g. Xu et al., 2013). It is also unknown how the high-TAlk water inputs (from the Yellow River – Bohai Sea system) and the $CaCO_3$ cycle will affect localized acidification on interannual to decadal scales. These problems need future investigation.

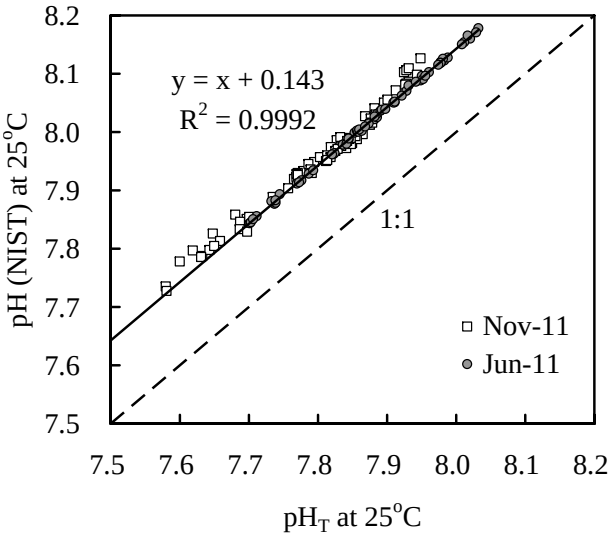

Fig. A1. Comparison between parallel pH measurements using total-hydrogen-ion scale pH buffers and NIST-traceable pH buffers.

Appendix A

Comparison between parallel pH measurements

Based on parallel measurements in June and November using two pH buffer sets, it was concluded that the pH data on the total-hydrogen-ion scale were lower than the NIST-traceable pH data by 0.143 ± 0.003 pH units (mean ±standard deviation, $n = 62$, based on the experiment in June) in the North Yellow Sea (Fig. A1).

Appendix B

Comparison between measured and calculated carbonate system parameters

To assess data quality, the calculated DIC (from field-measured pH at 25 °C and TAlk) versus measured DIC, calculated pH (from DIC and TAlk) versus field-measured pH, and Ω_{arag} values from DIC and TAlk versus those from field-measured pH (at 25 °C) and TAlk were compared. Most were consistent with each other at satisfactory deviation levels of $\pm 15\,\mu mol\,kg^{-1}$ (DIC), ±0.05 (pH) and ±0.1 (Ω_{arag}). Some Ω_{arag} values from DIC and TAlk were slightly higher than those from field-measured pH (at 25 °C) and TAlk by 0.1 to 0.2 (Fig. A2).

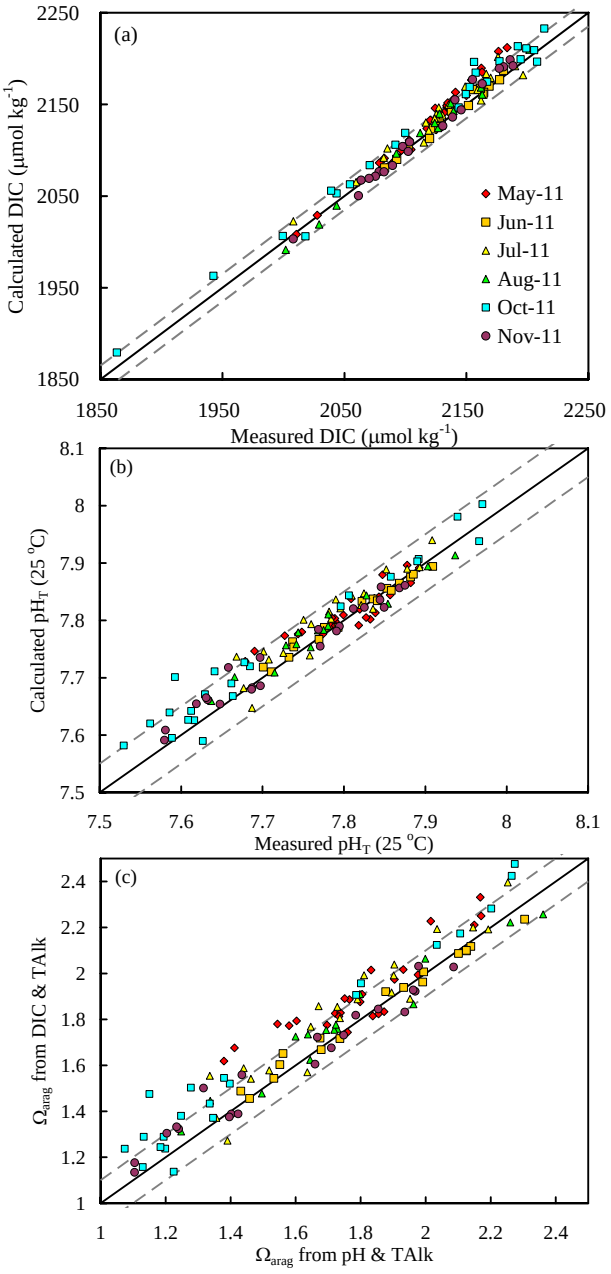

Fig. A2. Comparisons between calculated DIC (from measured pH at 25 °C and TAlk) and measured DIC data **(a)**, between calculated pH (from DIC and TAlk) and measured pH data **(b)**, and between calculated Ω_{arag} values from pH/TAlk and those from DIC/TAlk **(c)**. Unbroken lines are 1 : 1 lines, dashed lines denote deviation levels of $\pm 15\,\mu mol\,kg^{-1}$ **(a)**, ±0.05 pH units **(b)**, and ±0.1 Ω_{arag} **(c)**. Note that the precisions of DIC and pH determination were estimated at $\pm 2\,\mu mol\,kg^{-1}$ (Cai et al., 2004) and ±0.003 pH units (in correspondence with the precisions of potential determination of ±0.1 mV), respectively. The overall uncertainty of the measured pH_T data was estimated to be 0.01 pH units (Marion et al., 2011; Zhai et al., 2012). Primary data are presented in the Supplement for public reference.

Supplementary material related to this article is available online at http://www.biogeosciences.net/11/1103/2014/bg-11-1103-2014-supplement.pdf.

Acknowledgements. We thank L.-G. Guo, D. Qi, L. Sun and Y. Wang for data collection, D.-L. Wang for constructive discussion on the early manuscript, and C. Watts for her assistance with English. H.-J. Wang, X. Huang, Y.-W. Jiang, M.-H. Li and the crews of R/V *Dongfanghong 2* and R/V *Yixing* provided much help during the sampling surveys. Valuable comments and careful editing from K.-K. Liu, H. Thomas, and two anonymous reviewers have greatly improved the quality of this paper. The research was jointly supported by the National Natural Science Foundation of China (NSFC) (41276061 and 41076044) and the National Basic Research Program of China (2009CB421204). Sampling surveys were separately supported by the pilot project of the State Oceanic Administration of China (SOA) on air–sea carbon dioxide flux monitoring in the North Yellow Sea in May, July, October 2011, and January 2012; by the NSFC Open Ship-time projects in June, November 2011, and May 2012; and by the SOA project on marine environmental assessment method (contract DOMEP-MEA-01-10) in August 2011.

Edited by: K.-K. Liu

References

Andersen, S., Grefsrud, E. S., and Harboe, T.: Effect of increased pCO_2 level on early shell development in great scallop (Pecten maximus Lamarck) larvae, Biogeosciences, 10, 6161–6184, doi:10.5194/bg-10-6161-2013, 2013.

Baumann, H., Talmage, S. C., and Gobler, C. J.: Reduced early life growth and survival in a fish in direct response to increased carbon dioxide, Nat. Climatic Change, 2, 38–41, 2012.

Benson, B. B. and Krause, D.: The concentration and isotopic fractionation of oxygen dissolved in fresh water and seawater in equilibrium with the atmosphere, Limnol. Oceanogr., 29, 620–632, 1984.

Borges, A. V. and Gypens, N.: Carbonate chemistry in the coastal zone responds more strongly to eutrophication than to ocean acidification, Limnol. Oceanogr., 55, 346–353, 2010.

Briffa, M., de la Haye, K., and Munday, P. L.: High CO_2 and marine animal behaviour: Potential mechanisms and ecological consequences, Mar. Pollut. Bull., 64, 1519–1528, 2012.

Byrne, R. H., Mecking, S., Feely, R. A., and Liu, X.: Direct observations of basin-wide acidification of the North Pacific Ocean, Geophys. Res. Lett., 37, L02601, doi:10.1029/2009GL040999, 2010.

Cai, W.-J., Hu, X.-P., Huang, W.-J., Murrell, M.-C., Lehrter, J. C., Lohrenz, S. E., Chou, W.-C., Zhai, W.-D., Hollibaugh, J. T., Wang, Y.-C., Zhao, P.-S., Guo, X.-H., Gundersen, K., Dai, M.-H., and Gong, G.-C.: Acidification of subsurface coastal waters enhanced by eutrophication, Nat. Geosci., 4, 766–770, 2011.

Cai, W.-J., Dai, M.-H., Wang, Y.-C., Zhai, W.-D., Huang, T., Chen, S.-T., Zhang, F., Chen, Z.-Z., and Wang, Z.-H.: The biogeochemistry of inorganic carbon and nutrients in the Pearl River estuary and the adjacent Northern South China Sea, Cont. Shelf Res., 24, 1301–1319, 2004.

Caldeira, K. and Wickett, M. E.: Anthropogenic carbon and ocean pH, Nature, 425, 365, 2003.

Cao, Z.-M., Dai, M.-H., Zheng, N., Wang, D.-L., Li, Q., Zhai, W.-D., Meng, F.-F., and Gan, J.-P.: Dynamics of the carbonate system in a large continental shelf system under the influence of both a river plume and coastal upwelling, J. Geophys. Res., 116, G02010, doi:10.1029/2010JG001596, 2011.

Chen, C.-T. A.: Chemical and physical fronts in the Bohai, Yellow and East China seas, J. Mar. Syst., 78, 394–410, 2009.

Chen, C.-T. A. and Wang, S.-L.: Carbon, alkalinity and nutrient budget on the East China Sea continental shelf, J. Geophys. Res., 104, 20675–20686, 1999.

Chou, W.-C., Gong, G.-C., Hung, C.-C., and Wu, Y.-H.: Carbonate mineral saturation states in the East China Sea: present conditions and future scenarios, Biogeosciences, 10, 6453–6467, doi:10.5194/bg-10-6453-2013, 2013.

Dai, M.-H., Guo, X.-H., Zhai, W.-D., Yuan, L.-Y., Wang, B.-W., Wang, L.-F., Cai, P.-H., Tang, T.-T., and Cai, W.-J.: Oxygen depletion in the upper reach of the Pearl River estuary during a winter drought, Mar. Chem., 102, 159–169, 2006.

DeGrandpre, M. D., Hammar, T. R., Wallace, D. W. R., and Wrick, C. D.: Simultaneous mooring-based measurements of seawater CO_2 and O_2 off Cape Hatteras, North Carolina, Limnol. Oceanogr., 42, 21–28, 1997.

Dias, B. B., Hart, M. B., Smart, C. W., and Hall-Spencer, J. M.: Modern seawater acidification: the response of foraminifera to high-CO_2 conditions in the Mediterranean Sea, J. Geol. Soc. London, 167, 843–846, doi:10.1144/0016-76492010-050, 2010.

Dickson, A. G., Sabine C. L., and Christian J. R.: Guide to best practices for ocean CO_2 measurements, PICES Spec. Publ., No.3, 2007.

Dickson, A. G.: Standard potential of the reaction: AgCl(s) + 1/2 H_2(g) = Ag(s) + HCl(aq), and the standard acidity constant of the ion HSO_4^- in synthetic sea water from 273.15 to 318.15 K, J. Chem. Thermodyn., 22, 113–127, 1990.

Domenici, P., Allan, B., McCormick, M. I., and Munday, P. L.: Elevated carbon dioxide affects behavioural lateralization in a coral reef fish, Biol. Lett., 8, 78–81, 2012.

Doney, S. C., Fabry, V. J., Feely, R. A., and Kleypas, J. A.: Ocean acidification: the other CO_2 problem, Annu. Rev. Mar. Sci., 1, 169–192, 2009.

Du, B., Zhang, Y.-J., Shan, Y.-C., and Wang, H.: The characteristics of cold water mass variation at the bottom of the North Yellow Sea and its hydrological effects on the mortality of shellfish cultured in the waters of outer Chang-Shan Islands, Mar. Sci. Bull., 15 (4), 17–28, 1996 (in Chinese).

Duarte, C. M., Hendriks, I., E., Moore, T. S., Olsen, Y. S., Steckbauer, A., Ramajo, L., Carstensen, J., Trotter, J. A., and McCulloch, M.: Is ocean acidification an open-ocean syndrome? Understanding anthropogenic impacts on seawater pH, Estuar. Coast., 36, 221–236, 2013.

Feely, R. A., Sabine, C. L., Byrne, R. H., Millero, F. J., Dickson, A. G., Wanninkhof, R., Murata, A., Miller, L. A., and Greeley, D.: Decadal changes in the aragonite and calcite saturation state of the Pacific Ocean, Global Biogeochem. Cy., 26, GB3001, doi:10.1029/2011GB004157, 2012.

Feely, R. A., Alin, S. R., Newton, J., Sabine, S. L., Warner, M., Devol, A., Krembs, C., and Maloy, C.: The combined effects of ocean acidification, mixing, and respiration on pH and carbonate saturation in an urbanized estuary, Estuar. Coast. Shelf Sci., 88, 442–449, 2010.

Feely, R. A., Sabine, C. L., Hernandez-Ayon, J. M., Ianson, D., and Hales, B.: Evidence for upwelling of corrosive "acidified" water onto the continental shelf, Science, 320, 1490–1492, 2008.

Feely, R. A., Sabine, C. L., Lee, K., Millero, F. J., Lamb, M. F., Greeley, D., Bullister, J. L., Key, R. M., Peng, T.-H., Kozyr, A., Ono, T., and Wong, C. S.: In situ calcium carbonate dissolution in the Pacific Ocean, Global Biogeochem. Cy., 16, 1144, doi:10.1029/2002GB001866, 2002.

Friis, K., Körtzinger, A., and Wallace, D. W. R.: The salinity normalization of marine inorganic carbon chemistry data, Geophys. Res. Lett., 30, 1085, doi:10.1029/2002GL015898, 2003.

Gao, K.-S., Aruga, Y., Asada, K., Ishihara, T., Akano, T., and Kiyohara, M.: Calcification in the articulated coralline alga *Carollina pilulifera*, with special reference to the effect of elevated CO_2 concentration, Mar. Biol., 117, 129–132, 1993.

Gao, Y. and Li, Z.-Y.: Spatial and seasonal variation of chlorophyll and primary productivity in summer and winter in the Northern Yellow Sea, J. Ocean Univ. China, 39, 604–610, 2009 (in Chinese).

Gieskes, J. M.: Effect of temperature on the pH of seawater, Limnol. Oceanogr., 14, 679–685, 1969.

Gong, G.-C., Wen, Y.-H., Wang, B.-W., and Liu, G.-J.: Seasonal variation of chlorophyll *a* concentration, primary production and environmental conditions in the subtropical East China Sea, Deep-Sea Res. Pt. II, 50, 1219–1236, 2003.

Green, M. A., Waldbusser, G. G., Reilly, S. L., Emerson, K., and O'Donnell, S.: Death by dissolution: Sediment saturation state as a mortality factor for juvenile bivalves, Limnol. Oceanogr., 54, 1037–1047, 2009.

Gruber, N., Hauri, C., Lachkar, Z., Loher, D., Frölicher, T. L., and Plattner G. K.: Rapid progression of ocean acidification in the California current system, Science, 337, 220–223, 2012.

He, H.-C. and Yu, K.: The Yellow Sea, in: China Physical Geography Series – Chinese Marine Geography, edited by: Wang, Y., Liu, R.-Y., and Su, J.-L., Science Press, Beijing, 539–574, 2013 (in Chinese).

He, X., Bai, Y., Pan, D., Chen, C.-T. A., Cheng, Q., Wang, D., and Gong, F.: Satellite views of the seasonal and interannual variability of phytoplankton blooms in the eastern China seas over the past 14 yr (1998–2011), Biogeosciences, 10, 4721–4739, doi:10.5194/bg-10-4721-2013, 2013.

Hsueh, Y.: Recent current observations in the eastern Yellow Sea, J. Geophys. Res., 93, 6875–6884, 1988.

Huang, W.-J., Wang, Y.-C., and Cai, W.-J.: Assessment of sample storage techniques for total alkalinity and dissolved inorganic carbon in seawater, Limnol. Oceanogr. Methods, 10, 711–717, 2012.

Kelly, R. P., Foley, M. M., Fisher, W. S., Feely, R. A., Halpern, B. S., Waldbusser, G. G., and Caldwell, M. R.: Mitigating local causes of ocean acidification with existing laws, Science, 332, 1036–1037, 2011.

Lee, K., Tong, L. T., Millero, F. J., Sabine, C. L., Dickson, A. G., Goyet, C., Park, G. H., Wanninkhof, R., Feely, R. A., and Key, R. M.: Global relationships of total alkalinity with salinity and temperature in surface waters of the world's oceans, Geophys. Res. Lett., 33, L19605, doi:10.1029/2006GL027207, 2006.

Lenton, A., Metzl, N., Takahashi, T., Kuchinke, M., Matear, R. J., Roy, T., Sutherland, S. C., Sweeney, C., and Tilbrook, B.: The observed evolution of oceanic pCO_2 and its drivers over the last two decades, Global Biogeochem. Cy., 26, GB2021, doi:10.1029/2011GB004095, 2012.

Lewis, E. and Wallace D. W. R.: Program developed for CO_2 system calculations, ORNL/CDIAC-105, Carbon Dioxide Information Analysis Center, Oak Ridge National Laboratory, US Department of Energy, Oak Ridge, Tennessee, 1998.

Liu, W.-G. and He, M.-X.: Effects of ocean acidification on the metabolic rates of three species of bivalve from southern coast of China, Chinese J. Oceanol. Limnol., 30, 206–211, 2012.

Liu, Q. and Liu, Y.-J.: On export fluxes of several heavy metals in the Yalujiang Estuary, Mar. Environ. Sci., 11, 19–27, 1992 (in Chinese).

Long, X., Ma, Y.-R., and Qi, L.-M.: In vitro synthesis of High Mg calcite under ambient conditions and its implication for biomineralization process, Cryst. Growth Des., 11, 2866–2873, 2011.

Mao, X.-Y., Jiang, W.-S., Zhao, P., and Gao, H.-W.: A 3-D numerical study of salinity variations in the Bohai Sea during the recent years, Cont. Shelf Res., 28, 2689–2699, 2008.

Marion, G. M., Millero, F. J., Camões, M. F., Spitzer, P., Feistel, R., and Chen, C.-T. A.: pH of seawater, Mar. Chem., 126, 89–96, 2011.

Miao, J.-B., Liu, X.-Q., and Hsueh, Y.: Study of the formational mechanism of the Northern Yellow (Huanghai) Sea Cold Water Mass (I) – Solution of the model, Sci. China Ser. B, 34, 963–976, 1991.

Millero, F. J., Graham, T. B., Huang, F., Bustos-Serrano, H., and Pierrot, D.: Dissociation constants of carbonic acid in seawater as a function of salinity and temperature, Mar. Chem., 100, 80–94, 2006.

Morse, J. W., Arvidson, R. S., and Lüttge, A.: Calcium carbonate formation and dissolution, Chem. Rev., 107, 342–381, 2007.

Morse, J. W., Andersson, A. J., and Mackenzie, F. T.: Initial responses of carbonate-rich shelf sediments to rising atmospheric pCO_2 and "ocean acidification": Role of high Mg-calcites, Geochim. Cosmochim. Acta, 70, 5814–5830, 2006.

Mucci, A.: The solubility of calcite and aragonite in seawater at various salinities, temperatures, and one atmosphere total pressure, Am. J. Sci., 283, 780–799, 1983.

Munday, P. L., Dixson, D. L., McCormick, M. I., Meekan, M., Ferraric, M. C. O., and Chivers D. P.: Replenishment of fish populations is threatened by ocean acidification, P. Natl. Acad. Sci. USA, 107, 12930–12934, 2010.

Munday, P. L., Dixson, D. L., Donelson, J. M., Jones, G. P., Pratchett, M. S., Devitsina, G. V., and Døving, K. B.: Ocean acidification impairs olfactory discrimination and homing ability of a marine fish, P. Natl. Acad. Sci. USA, 106, 1848–1852, 2009.

Orr, J. C., Fabry, V. J., Aumont, O., Bopp, L., Doney, S. C., Feely, R. A., Gnanadesikan, A., Gruber, N., Ishida, A., Joos, F., Key, R. M., Lindsay, K., Maier-Reimer, E., Matear, R., Monfray, P., Mouchet, A., Najjar, R. G., Plattner, G.-K., Rodgers, K. B., Sabine, C. L., Sarmiento, J. L., Schlitzer, R., Slater, R. D., Totterdell, I. J., Weirig, M.-F., Yamanaka, Y., and Yool, A.: Anthropogenic ocean acidification over the twenty-first century and its impacts on calcifying organisms, Nature, 437, 681–686, 2005.

Parsons, T. R., Yoshiaki, M., and Lalli, C. M.: A manual of chemical and biological methods for seawater analysis, Pergamon Press, Oxford, 1984.

Pelletier, G. J., Lewis, E., and Wallace, D. W. R.: CO2SYS.XLS: A calculator for the CO_2 system in seawater for Microsoft Excel/VBA, Ver. 16, Washington State Department of Ecology, Olympia, Washington, 2011.

Qiao, F.-L., Watanabe, M., Yuang, Y.-L., and Wan, Z.-W.: Simulation of Circulation in the Yellow Sea and East China Sea, J. Hydrodynamics Ser. A, 13, 244–254, 1998 (in Chinese).

Redfield, A. C., Ketchum, B. H., and Richards, F. A.: The influence of organisms on the composition of seawater, in: The Sea, Vol. 2, edited by: Hill, M. N., John Wiley and Sons, New York, 26–77, 1963.

Sabine, C. L., Feely, R. A., Gruber, N., Key, R. M., Lee, K., Bullister, J. L., Wanninkhof, R., Wong, C. S., Wallace, D. W. R., Tilbrook, B., Millero, F. J., Peng, T.-H., Kozyr, A., Ono, T., and Rios, A. F.: The oceanic sink for anthropogenic CO_2. Science, 305, 367–371, 2004.

Salisbury, J., Green, M., Hunt, C., and Campbell, J.: Coastal acidification by rivers: A threat to shellfish?, EOS Trans. Am. Geophys. Union, 89, 513, 2008.

Shamberger, K. E. F., Feely, R. A., Sabine, C. L., Atkinson, M. J., DeCarlo, E. H., Mackenzie, F. T., Drupp, P. S., and Butterfield, D. A.: Calcification and organic production on a Hawaiian coral reef, Mar. Chem., 127, 64–75, 2011.

State Oceanic Administration of China: Bulletin of Marine Environmental Status of China in 2011, http://www.soa.gov.cn/zwgk/hygb/, last access date: 2014-02-22, 2012 (in Chinese).

Steuber, T. and Rauch, M.: Evolution of the Mg / Ca ratio of Cretaceous seawater: Implications from the composition of biological low-Mg calcite, Mar. Geol., 217, 199–213, 2005.

Sunda, W. G. and Cai, W.-J.: Eutrophication induced CO_2-acidification of subsurface coastal waters: interactive effects of temperature, salinity, and atmospheric pCO_2, Environ. Sci. Technol., 46, 10651–10659, 2012.

Sundquist, E. T., Plummer, L. N., and Wigley, T. M. L.: Carbon dioxide in the ocean surface: the homogenous buffer factor, Science, 204, 1203–1205, 1979.

Sweeney, C., Gloor, E., Jacobson, A. R., Key, R. M., McKinley, G., Sarmiento, J. L., and Wanninkhof, R.: Constraining global air-sea gas exchange for CO_2 with recent bomb ^{14}C measurements, Global Biogeochem. Cy., 21, GB2015, doi:10.1029/2006GB002784, 2007.

Taguchi, F. and Fujiwara, T.: Carbon dioxide stored and acidified low oxygen bottom waters in coastal seas, Japan, Estuar. Coast. Shelf Sci., 86, 429–433, 2010.

Takahashi, T., Olafsson, J., Goddard, J. G., Chipman, D. W., and Sutherland, S. C.: Seasonal variation of CO_2 and nutrients in the high-latitude surface ocean: a comparative study, Global Biogeochem. Cy., 7, 843–878, 1993.

Tan, S.-C., Shi, G.-Y., Shi, J.-H., Gao, H.-W., and Yao, X.: Correlation of Asian dust with chlorophyll and primary productivity in the coastal seas of China during the period from 1998 to 2008, J. Geophys. Res., 116, G02029, doi:10.1029/2010JG001456, 2011.

Thomas, H., Prowe, A. E. F., van Heuven, S., Bozec, Y., de Baar, H. J. W., Schiettecatte, L.-S., Suykens, K., Koné, M., Borges, A. V., Lima, I. D., and Doney, S. C.: Rapid decline of the CO_2 buffering capacity in the North Sea and implications for the North Atlantic Ocean, Global Biogeochem. Cy., 21, GB4001, doi:10.1029/2006GB002825, 2007.

Turley, C. and Gattuso, J.-P.: Future biological and ecosystem impacts of ocean acidification and their socioeconomic-policy implications, Curr. Opin. Environ. Sustain., 4, 278–286, 2012.

Wang, H.-J., Yang, Z.-S., Saito, Y., Liu, J.-P., Sun, X.-X., and Wang Y.: Stepwise decreases of the Huanghe (Yellow River) sediment load (1950–2005): impacts of climate change and human activities, Global Planet. Chang., 57, 331–354, 2007.

Wang, Y.-C, Liu, Z., Gao, H.-W., Ju, L., and Guo, X.-Y.: Response of salinity distribution around the Yellow River mouth to abrupt changes in river discharge, Cont. Shelf Res., 31, 685–694, 2011.

Wang, X.-L., Zhang, L.-J., Su, Z., Li, Y., Zhang, X.-S., and Gao, H.-W.: The conservative and non-conservative behaviors of total alkalinity in the Huanghe estuary, J. Ocean Univ. China, 35, 1063–1066, 2005 (in Chinese).

Wanninkhof, R.: Relationship between wind speed and gas exchange over the ocean, J. Geophys. Res., 97, 7373–7382, 1992.

Wei, H., Tian, T., Zhou, F., and Zhao, L.: Numerical studies on the water exchange of the Bohai Sea: simulation of the half-life time by dispersion model, J. Ocean Uni. Qingdao, 32, 519–525, 2002 (in Chinese).

WMO/GAW: The state of greenhouse gases in the atmosphere based on global observations through 2011, WMO Greenhouse Gas Bulletin, No.8, 1–4, 2012.

Wong, G. T. F.: Removal of nitrite interference in the Winkler determination of dissolved oxygen in seawater, Mar. Chem., 130/131, 28–32, 2012.

Woosley, R. J., Millero, F. J., and Grosell, M.: The solubility of fish-produced high magnesium calcite in seawater, J. Geophys. Res., 117, C04018, doi:10.1029/2011JC007599, 2012.

Wu, D.-X., Mu, L., Li, Q., Bao, X.-W., and Wan, X.-Q.: Characteristics of long-term variations of sea water salinity in the Bohai Sea and the possible controls, Prog. Nat. Sci., 14, 191–195, 2004 (in Chinese).

Xia, B. and Zhang, L.-J.: Carbon distribution and fluxes of 16 rivers discharging into the Bohai Sea in summer, Acta Oceanol. Sin., 30 (3), 43–54, doi:10.1007/s13131-011-0118-3, 2011.

Xu, X.-M., Zhai, W.-D., and Wu, J.-H.: Effects of CO_2-driven ocean acidification on the calcification and respiration of *Ruditapes philippinarum*, Acta Oceanol. Sin., 35 (5), 112–120, 2013 (in Chinese).

Yamamoto, S., Kayanne, H., Terai, M., Watanabe, A., Kato, K., Negishi, A., and Nozaki, K.: Threshold of carbonate saturation state determined by CO_2 control experiment, Biogeosciences, 9, 1441–1450, doi:10.5194/bg-9-1441-2012, 2012.

Yamamoto-Kawai, M., McLaughlin, F. A., Carmack, E. C., Nishino, S., and Shimada, K.: Aragonite undersaturation in the Arctic Ocean: Effects of ocean acidification and sea ice melt, Science, 326, 1098–1100, 2009.

Yang, G.-P., Zhang, H.-H., Su, L.-P., and Zhou, L.-M.: Biogenic emission of dimethylsulfide (DMS) from the North Yellow Sea, China and its contribution to sulfate in aerosol during summer, Atmos. Environ., 43, 2196–2203, 2009.

Yuan, D.-L., Zhu, J.-R., Li, C.-Y., and Hu, D.-X.: Cross-shelf circulation in the Yellow and East China Seas indicated by MODIS satellite observations, J. Mar. Syst., 70, 134–149, 2008.

Zeebe, R. E. and Wolf-Gladrow, D.: CO_2 in seawater: Eqiulibrium, kinetics, isotopes, Elsevier Oceanography Series, 65, 346 pp., 2001.

Zhai, W.-D., Zhao, H.-D., Zheng, N., and Xu, Y.: Coastal acidification in summer bottom oxygen-depleted waters in northwestern-northern Bohai Sea from June to August in 2011, Chinese Sci. Bull., 57, 1062–1068, 2012.

Zhai, W. D., Dai, M., and Cai, W.-J.: Coupling of surface pCO_2 and dissolved oxygen in the northern South China Sea: impacts of contrasting coastal processes, Biogeosciences, 6, 2589–2598, doi:10.5194/bg-6-2589-2009, 2009.

Zhang, J.: Impact of drainage basin weathering upon riverine chemistry, in: Biogeochemical Studies of Major Chinese Estuaries – Element Transfer and Environment, edited by: Zhang, J., China Ocean Press, Beijing, 1–15, 1997 (in Chinese).

Zhang, J., Yu, Z.-G., Liu, S.-M., Xu, H., and Liu, M.-G.: Dynamics of nutrient elements in three estuaries of North China: the Luanhe, Shuangtaizihe, and Yalujiang, Estuaries, 20, 110–123, 1997.

Zhang, J.: Nutrient elements in large Chinese estuaries, Cont. Shelf Res., 16, 1023–1045, 1996.

Zhang, J.: Atmospheric wet deposition of nutrient elements: correlation with harmful biological blooms in Northwest Pacific coastal zones, Ambio, 23, 464–468, 1994.

Zhang, S.-W., Xia, C.-S., and Yuan, Y.-L.: A physical-biochemical coupling model of Yellow Sea cold water mass, Prog. Nat. Sci., 12, 315–319, 2002 (in Chinese).

Zhao, B.-R.: A study of the circulations of the northern Yellow Sea cold water mass – Effects of tidal mixing on them, Oceanol. Limnol. Sin., 27, 429–435, 1996 (in Chinese).